Modeling Accurate Human Activity Recognition for Embedded Devices Using Multi-level Distillation

Runze Chen, *Graduate Student Member, IEEE*, Haiyong Luo, *Member, IEEE*, Fang Zhao, *Member, IEEE*, Xuechun Meng, Zhiqing Xie, and Yida Zhu

Abstract—Human Activity Recognition (HAR) based on IMU sensors is a crucial area in ubiquitous computing. Because of the trend of deploying AI on IoT devices or smartphones, more researchers are designing different HAR models for embedded devices. Deployment of models in embedded devices can help enhance the efficiency of HAR. We propose a multi-level HAR modeling pipeline called Stage-Logits-Memory Distillation (SMLDist) for constructing deep convolutional HAR models with embedded hardware support. SMLDist includes stage distillation, memory distillation, and logits distillation. Stage distillation constrains the learning direction of the intermediate features. The teacher model teaches the student models how to explain and store the inner relationship among high-dimensional features based on Hopfield networks in memory distillation. Logits distillation builds logits distilled by a smoothed conditional rule to preserve the probability distribution and enhance the softer target accuracy. We compare the accuracy, F1 macro score, and energy cost on embedded platforms of a MobileNet V3 model built by SMLDist with various state-of-the-art HAR frameworks. The product model has a good balance with robustness and efficiency. SMLDist can also compress models with a minor performance loss at an equal compression ratio to other advanced knowledge distillation methods on seven public datasets.

Index Terms—human activity recognition, knowledge distillation, artificial neural network, time sequence, embedded software

1 Introduction

CCURATELY recognizing the activities and behaviors of users plays an essential role in ubiquitous computing. It is impossible for an HAR system to operate independently without sensors. Smartphones or wearable devices integrate various sensors, including acceleration, gyroscope, magnetometer, and so on, to gain the ability to sense users' physical motion. The sensor-based human activity recognition (HAR) system analyzes users' movement and state of the environment to distinguish users' suitable activity. The users' HAR contexts express semantic information about their activity in real-time from the original sequence of the sensor signal. Information on user activities is a key context for many applications, such as smart homes [1], [2], human-computer interaction [3], health monitoring [4], [5], transportation schedules [6], [7], [8], etc. These applications require a real-time response with higher HAR accuracy.

Over the past few decades, the booming smartphone and mobile device market contains billions of users with a wealth of activity data [6], [9], [10]. Deep learning embodies excellent potential in an era of massive data growth. The deep learning technique provides a better generalization capability for recognizing human activities. Emerging HAR methods based on deep learning have lots of delicate struc-

(Corresponding author: Haiyong Luo and Fang Zhao.)

ture to improve the accuracy of HAR. The earlier idea of designing HAR models is the fusion of multi-positional, temporal and spectral features extracted from the sensor's raw signals. The combination of convolutional neural networks (CNN) and residual neural networks (RNN) is the most traditional way to fuse spatial and temporal features in the HAR model [11]. The attention mechanism [12], [13] provides HAR methods with new ideas to enrich multipositional sensor features' expression [14], [15], [16]. The architecture of embracement layers [17], [18] provides a brandnew operation to combine sensor features with multiple modalities in HAR tasks. Some HAR methods also focus on spectral expressions in deep neural networks. These HAR techniques [14], [16], [19], [20] apply fast Fourier transform (FFT) to the raw sensor signals and use spectral representations to classify human activities. Independent recurrent neural networks (IndRNN) [21] improve the mechanism of RNN and prevent problems of gradient vanishing and exploding. The integration of IndRNN layers in HAR models can assist sufficiently in expressing temporal features with a deeper structure [19], [20]. Hopfield networks [22] integrate synaptic connection patterns with energy-based updating rules. Modern Hopfield networks [23] working with deep networks can help to store the global relations among different high-dimensional features. Various activities have different implicit structural knowledge in the high-dimensional representation. Hopfield networks can represent structural knowledge as relation patterns, which linear units cannot support [22], [23].

HAR model designing, which focuses on fusing various types of feature representations, provides many innovative ideas. Dedicated neural network architectures tend

R. Chen, F. Zhao, X. Meng, Z. Xie and Y. Zhu are with the School of Computer Science (National Pilot Software Engineering School), Beijing University of Posts and Telecommunications, Beijing 100876, China. E-mail: {chenrz925,zfsse,mxc,xzq0112,dozenpiggy}@bupt.edu.cn

H. Luo is with the Beijing Key Laboratory of Mobile Computing and Pervasive Device, Institute of Computing Technology, Chinese Academy of Sciences, Beijing 100190, China E-mail: yhluo@ict.ac.cn

to have more parameters and operations. It means these techniques need more computational overheads and larger memory bandwidths. System designers have to deploy these computation-intensive models into a cloud server and acquire the models via network connections. Continuous real-time HAR requires mobile devices and cloud servers to keep a steady network connection to transfer sensor commands and values. Steady network connections require higher energy costs and the ideal network environment. The computing performance of mobile devices on the world market is improving significantly. It enables mobile devices to predict using neural networks. Over the past few years, HAR models are ready for deployment on modern mobile devices. HAR models must be sufficiently efficient and lightweight to be adapted to the embedded device environment.

To build more lightweight models, many researchers [24], [25], [26] focus on the balance between the performance and efficiency of deep models. Efficient deep neural networks [24] and model compression methods [25], [26] emerge to build deep models with less computational overheads and similar performance. Knowledge distillation (KD) is a method to distill knowledge from a more extensive network into a small network. By mimicking the teacher model, student models can achieve similar accuracy and instantaneity with less computational overhead. G. Hinton et al. [27] introduces the original KD method to distill the teacher model's response knowledge. It encourages more researchers to focus on knowledge distillation. Some knowledge distillation methods, including feature-based KD methods [28], [29] and structure-based methods [30], try to transfer hidden features or weights as knowledge to student models.

Different from the previous study, we propose a multilevel distillation pipeline for HAR modeling called Stage-Memory-Logits distillation (SMLDist). SMLDist provides full-level distillation to decrease the performance loss in model compression. In deep neural networks, stacked convolutional operations are the most fundamental structure. Moreover, it is easy to perform convolutional operations in parallel. Therefore, SIMD instructions [31] of embedded devices can optimize those convolutional operations. SMLDist aims to build a KD-based pipeline to construct lightweight and powerful deep convolutional models for low-power devices. It includes three levels of knowledge distillation: stage distillation, memory distillation, and logits distillation. Stage distillation constrains the intermediate representations of the student models strictly. We integrate the memory units based on Hopfield networks as the final stage of the whole architecture. The pipeline distills the memories in Self-adaptive Memory-Intuition Units (SIMU) from teachers to students. After mapping penultimate representations to the final logits, we use an optimized logits distillation strategy to enrich the information of one-hot encoded labels. By conducting experiments on seven public human activity recognition datasets, we evaluate the performance of models powered by SMLDist. A series of experiments prove that these models can maintain ideal performance and good efficiency on mobile embedded devices by reducing model computing overhead and memory bandwidth. Also, the

source code of SMLDist is available online.1

We summarize the main contributions of SMLDist as follows:

- SMLDist is a multi-level knowledge distilling pipeline that covers the entire process of training a HAR model. SMLDist consists of stage distillation, memory distillation, and logits distillation. Stage distillation constrains the fundamental learning direction of representation. Memory distillation guides the student models on how to explain the relationship between high-dimensional features. Logits distillation transfers the implicit probability of activities to the student models.
- We design a self-adaptive strategy to balance the intuition branch and the memory branch in SIMU. SIMU uses a self-adapted weight to balance the memory branch and the intuition branch in the training process. After the training process, SIMU prunes the branch with a smaller weight and uses the branch with a larger weight to predict in the evaluating mode. Memory distillation shares the memory of teacher models to their students. The teacher models share parameters of the two branches of SMIU with their student models.
- We evaluate a variety of state-of-the-art models and KD methods on seven mainstream public HAR datasets. We conduct a complete evaluation and comparison of accuracy, F1 macro score, number of parameters, operations, as well as the energy cost on the real embedded device on those datasets. The experiments display the characteristics of those KD methods and model frameworks on the HAR problems, which can be an objective reference criterion for other researchers.

The remainder of this paper is organized as follows. Section 2 introduces related works of human activity recognition and knowledge distilling. Section 3 introduces methods of SMLDist. In Section 4, we perform experiments to evaluate the availability and performance of methods in SMLDist. We make conclusions and introduce future work about this paper in Section 5.

2 RELATED WORK

Many researchers focus on the domain of HAR and make great progress, including the new architecture of deep learning models and software to recognize human activities. As applications on embedded devices of deep neural models have significant growth, researchers need to design more efficient and eco-friendly deep models. Knowledge distillation is an essential part of model compression, with lots of innovations in recent years.

Deep learning techniques boost the development of HAR solutions. Since the raw signals of the sensors have temporal sequence characteristics, many researchers use techniques to extract spatial, temporal and spectral features. DeepConvLSTM [11] provides a classical method that performs convolutional operations on each time window

to extract spatial features and uses two layers of LSTM to extract temporal features. HAR models use the attention mechanism [12], [13] to combine spatial features and temporal features. AttnSense [14] provides a model with CNN modules and GRU modules combined by the attention mechanism. SparseSense [15] uses sample embedding and segment embedding based on linear operations to recognize human activities. The model of SparseSense learns directly from sparse data using a deep learning paradigm in an end-to-end manner. Researchers also commonly focus on spectral features of sensor signals. IndRNN [21] is a new architecture of RNNs with the recurrent connection formulated as a Hadamard product, of which neurons in the same layer are independent and connected across layers. B. Zhao et al. [19], [20] apply the IndRNN module to HAR problems. They use all temporal features and spectral features computed by FFT (Fast Fourier Transform). They combine spectral and temporal features and feed them into IndRNN layers to perceive the long-term human activity pattern. J.-H. Choi et al. [17], [18] design EmbraceNet to extract correlated information between different modalities of sensors. S. Liu et al. [16] integrate global attention mechanisms into convolutional networks to combine high-level node features and use GRU modules to enable temporal perception.

Most HAR methods design a variety of architectures to analyze spatial, temporal, and spectral models in raw sensor signals to enhance the recognition performance of human activities. However, exquisite architecture may result in a larger scale and higher energy costs for the models. As embedded devices' computational ability get gradually mature, embedded devices can provide the platform to deploy end-to-end deep learning models and support real-time inference. Deploying deep neural models of mobile devices is a realistic and reasonable mission for AI researchers. Human activity recognition is an eligible application of mobile devices with MEMS sensors. To deploy a deep HAR model on mobile wearable devices, model compression with small accuracy diminution is a critical and challenging mission. Universally, model compression methods include pruning [32], [33], [34], [35], [36], quantization [37], [38], lowrank approximation & sparsity [39], [40], and knowledge distillation [27], [41], [42]. Model pruning aims to prune non-significant weights in large models, and those pruned large-sparse models also have significant performance [43]. We can divide model pruning into structured pruning [32], [33] and unstructured pruning [34], [35], [36]. The most intuitive difference between those two types of pruning is the atomicity of dropped elements' fundamental units. Structured pruning removes whole layers or channels in the deep models, and unstructured pruning removes weights or neurons. Model pruning aims to decrease the number of operations or weights in models, but quantization aims to reduce the bit-width of the data flowing through the models [26]. The data objects in a deep neural model include weight [44], [45], [46], activation [44], [45], [46], error [45], [46], gradient [37], [45], [47], etc. Many methods exploit the complementary action of model pruning and quantization. Deep learning frameworks, such as PyTorch [48], also provide quantization toolkits of models.

Knowledge distillation [27], [41], [42] plays a vital role in developing deep learning models which are friendly

to wearable embedded devices. According to the distilled elements in the deep models [25], we can divide KD into response-based KD [27], [42], feature-based KD [41], [41], [49], and relation-based KD [50], [51]. Hinton et al. [27] formally popularize the idea of knowledge distillation in 2015. The vanilla knowledge distillation transfers the logits in the teacher-student architecture. The transferred logits as the soft target and the one-hot hard label constrain the back-forwarding process of student models. However, the soft targets from teacher models are not always correct. The wrong soft target may mislead student models. Z. Meng et al. [42] design a conditional loss function, which uses the hard label instead of the soft target when the teacher model predicts incorrectly. Neurons or features of deep models' intermediate layers are another form of knowledge to be distilled. Xu et al. [41] analyze the relationship between logits distillation and label smoothing. They use a normalized feature distilling to improve the temperature mechanism of the vanilla knowledge distillation. Instead of distilling logits, methods distilling other knowledge emerge in recent years. Romero et al. [28] use hint feature distillation to compress wide and deep models into thinner and deeper ones. Neuron Selectivity Transfer [52] uses MMD loss [53] to metric the distance between the hint features in the teacher and student models. Similarity-Preserving KD [29] distills the similarity matrix of intermediate neurons from the teacher to the student. Factor Transfer [54] designs an encoder-decoder-styled module to extract the factor of the teacher model's intermediate features and uses an encoder for the student model to mimic the factor from the teacher model.

Inspired by the idea of knowledge distillation, SMLDist tries to develop slim neural networks based on widely used deep architectures by distilling anchor features, response logits, and patterns in memory units from the massive convolutional networks. We use MobileNet V3 [24] to work as a backbone of deep learning architecture in this paper because of its efficiency. Abundant, powerful toolkits and frameworks [55], [56], [57], [58], [59], [60], [61] provided by communities are of great help to researchers.

3 THE PIPELINE OF SMLDIST

We present the proposed methods of Stage-Memory-Logits Distillation (SMLDist) in details in this section. We firstly introduce the problem definitions and notations. In the order of Stage-Memory-Logits Distillation, we will introduce stage distillation, memory distillation (with SIMU), and logits distillation in the following sections. Figure 1 displays the pipeline of stage distillation and logits distillation to build a model with three stages.

3.1 Problem Definition and Notation

We propose a HAR modeling method in this paper. HAR model is a function $f: \mathcal{X} \to \mathcal{Y}$ mapping the raw sensor signal vectors \mathcal{X} to the final class logits \mathcal{Y} , which is the most critical part of the whole method. We predict and classify human activity through the HAR method on each temporal window on the sensor signal. For example, for the i-th window in the whole dataset, the raw signal vectors

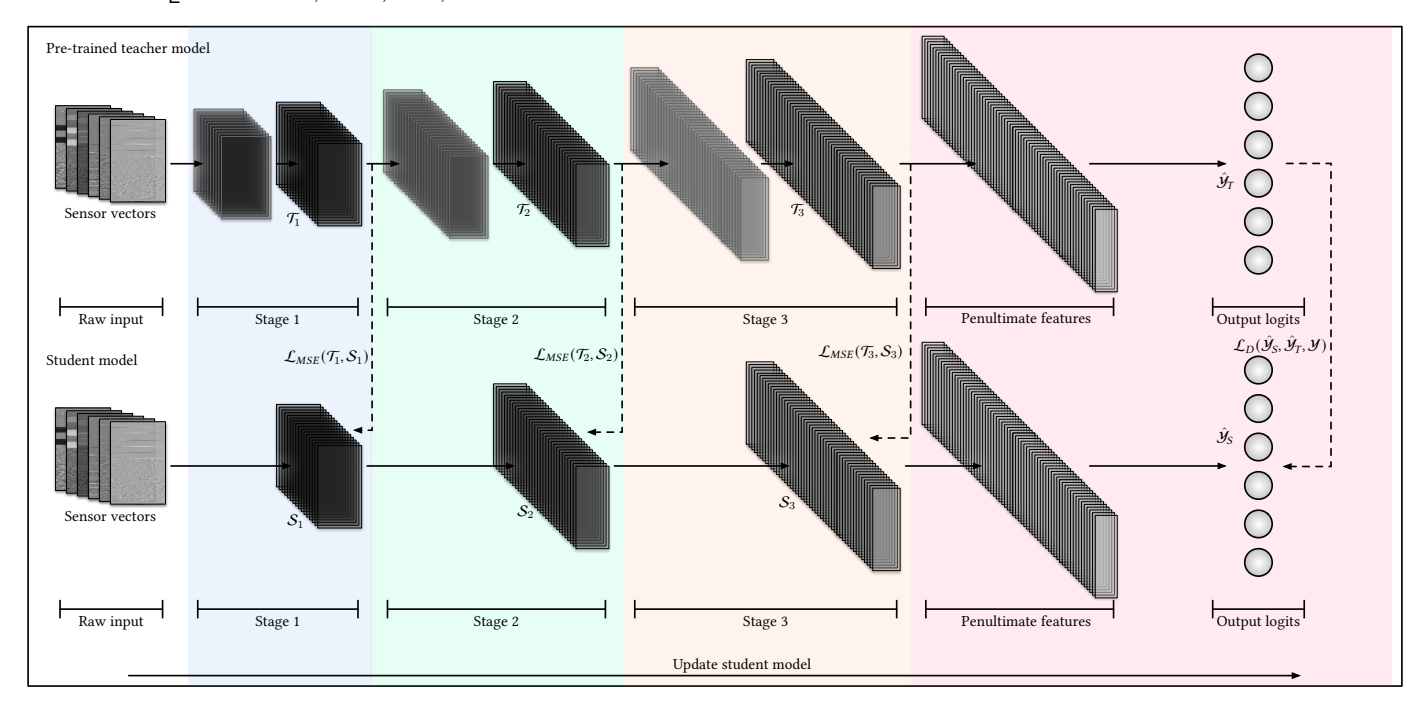


Fig. 1. Stage distillation and logits distillation

should be \mathcal{X}_{i} , and the class logits \mathcal{Y}_i . The collection of all participating human activity classification is $C = \{c_i\}_{i=1}^n$. We usually use the softmax function $\sigma(\cdot)$ to map the class logits \mathcal{Y} to the class probability vector $P = (P_{c_1}, \cdots, P_{c_n})$. To balance the HAR model's accuracy and efficiency, we perform stage knowledge distillation on the deep vanilla model and design the self-adaptive intuition-memory model to upgrade the model's recognition efficiency.

3.2 Stage Distillation

Stage distillation teaches the student model how to perceive and extract more features from the raw signals. In stage distillation, we divide the model into different stages, whose output features are anchor features. Each stage of the student model mimics the anchor features of the teacher model's corresponding stage strictly. As the stage target, the teacher model's intermediate features can constrain the convergence trend of intermediate layers in the student model. As an incremental training pipeline, stage distillation gradually activates the weights or neurons in layers of each stage.

Assume that a HAR model $f(\cdot)$ consists of n stages, such as Equation 1.

$$f(\cdot) = (f_1 \circ \cdots \circ f_n \circ h)(\cdot), \tag{1}$$

where the i-th stage $f_i(\cdot)$ extracts hidden features on different scales, and the final layer $h(\cdot)$ of the model decides to classify activities based on the knowledge extracted from previous stages. When i increases, the stage $f_i(\cdot)$ can perceive features on a larger temporal scale. The classifier uses the perceived features from the previous stages for the final classification.

As displayed in Figure 1, the feature \mathcal{T}_i produced by stage i of the teacher model guides the student model how

the corresponding stage extracts features S_i . In the teacher model f_T and the student model f_S , the i-th stage response features are as Equation 2 displays:

$$\mathcal{T}_i = (f_{T_1} \circ \dots \circ f_{T_i})(\mathcal{X}),$$

$$\mathcal{S}_i = (f_{S_1} \circ \dots \circ f_{S_i})(\mathcal{X}).$$
(2)

In stage distillation, anchor features \mathcal{T}_i from the teacher model constrain the corresponding features \mathcal{S}_i strictly by guiding the student stages $(f_{S_1} \circ \cdots \circ f_{S_i})(\cdot)$ to regress the mapping $\mathcal{X} \to \mathcal{T}_i$. The regressions of each stages use mean squared error (MSE) function, which is displayed in Equation 3.

$$L_{MSE}(\mathcal{T}_i, \mathcal{S}_i) = \text{mean}((\mathcal{S}_i - \mathcal{T}_i)^2), \quad i \in \{1, \dots, N\},$$
(3)

where the total number of stages in the distilling process is N, the anchor features of stage i provided by the teacher model is \mathcal{T}_i and the regressed features of stage i from the student model is \mathcal{S}_i . On each stage, the regression to the teacher decreases the distance between the teacher's anchor and the student's anchor in the feature space.

The front-end layers perceive the raw input data and map them into a more complex feature space to represent users' motion. In the feature space, the features should have a relationship with each other. Traditional linear units cannot represent the pattern of features' relationship well. So we design a more robust unit to map the features into final logits.

3.3 SIMU and Memory Distillation

We design the self-adaptive intuition-memory unit (SIMU) as displayed in Figure 2. Memory distillation in SIMU teaches the student models **how to build relationships**

Algorithm 1 The process of SMLDist.

Require: A collection of raw sensor vectors X, corresponding collection of hard labels Y, a pre-trained teacher model $f_T = f_{T_1} \circ f_{T_2} \circ \cdots \circ f_{T_n} \circ h_T$ with n stages, an optimizer method O_{Si} for distilling in stage i and an optimizer O_H for logits distilling.

Ensure: A slim student model $f_S = f_{S_1} \circ f_{S_2} \circ \cdots \circ f_{S_n} \circ h_S$.

1: Initialize a slim model $f_S = f_{S_1} \circ f_{S_2} \circ \cdots \circ f_{S_n} \circ h_S$ with the same shape of anchor features as the teacher model $f_T = f_{T_1} \circ f_{T_2} \circ \cdots \circ f_{T_n} \circ h_T$.

- 2: Block the teacher model f_T to avoid any gradient recording.
- 3: **for** stage $i=1,2,\cdots,n$ **do** \triangleright Feature distilling for each stage i.

```
Let F_T = f_{T_1} \circ \cdots \circ f_{T_i} and F_S = f_{S_1} \circ \cdots \circ f_{S_i}.
 4:
          for each epoch until F_S performs well do
 5:
               for each sample \mathcal{X},\mathcal{Y} in X,Y do
 6:
 7:
                    Renew the optimizer O_{Si}.
                    \mathcal{T}_i = F_T(\mathcal{X})
 8:
                    S_i = F_S(\mathcal{X})
 9
10:
                    Optimize
                                     and
                                                back-propagating
     O_{Si}(F_S, L_{MSE}(\mathcal{T}_i, \mathcal{S}_i), \nabla F_S).
               end for
11:
```

12: end for

13: end for

14: Transfer W_q , W_k , W_v , and W_h in SIMU from the teacher model to the student model. \triangleright Memory distilling.

15: **for** each epoch until f_S performs well **do** \triangleright Logits distilling for the whole student model.

```
for each sample \mathcal{X},\mathcal{Y} in X,Y do
16:
17:
                  Renew the optimizer O_T.
                  \hat{\mathcal{Y}}_T = f_T(\mathcal{X})
18:
                  \hat{\mathcal{Y}}_S = f_S(\mathcal{X})
19:
                  Optimize
20:
                                          and
                                                        back-propagating
                                                                                               using
      O_T(f_S, \mathcal{L}_D(\hat{\mathcal{Y}}_S, \hat{\mathcal{Y}}_T, \mathcal{Y}), \nabla f_S)
21:
            end for
```

22: end for 23: return f_S

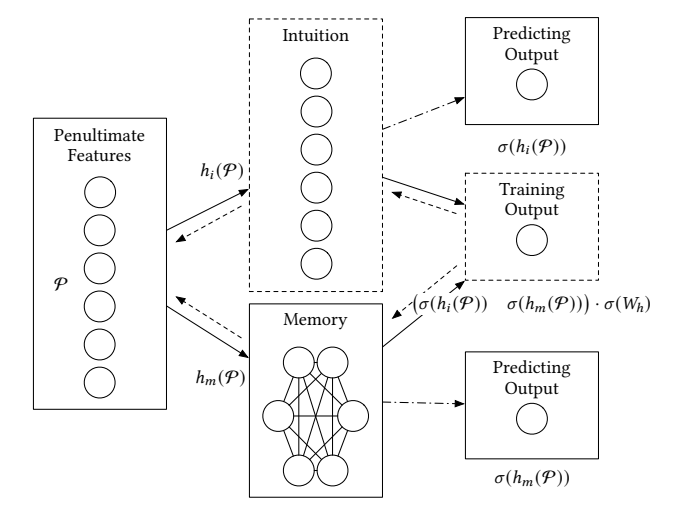


Fig. 2. Self-adaptive intuition-memory unit.

among various feature patterns in the feature space of the penultimate layer. The modern Hopfield network [23] in the deep learning architecture needs continuous interaction function. The lse (log-sum-exp) function

$$lse(\beta, x) = \beta^{-1} log(\sum_{i=1}^{N} exp(\beta x_i)),$$
 (4)

where $\beta > 0$, and N is the number of stored patterns $x_i \in \mathbb{R}^d$, constitutes a modern energy function [23] displayed in Equation 5.

$$E(x) = -\operatorname{lse}(\beta, x^{T}\xi) + \frac{1}{2}\xi^{T}\xi + \beta^{-1}\log N + \frac{1}{2}N^{2}, \quad (5)$$

where the stored relationship pattern $x_i \in \mathbb{R}^d$ represented by $X = (x_1, \dots, x_N)$, $\xi \in \mathbb{R}^d$ is the state pattern of the Hopfield network. And the update rule of the state pattern is

$$\xi_{new} = X\sigma(\beta X^T \xi). \tag{6}$$

In the deep learning architecture, the update rule in Equation 6 could be simplified and implemented as Equation 7.

$$Z = \sigma(\beta X W_q W_k^T X^T) X W_v, \tag{7}$$

where X is the Hopfield layer's input, the output Z is a set of vectors with the same shape as X, and the matrices W_k , W_v and W_q are different weights in the Hopfield layer.

The Hopfield layer can storage global relationship patterns of human activities from training sets. We implement the Hopfield layer as the memory branch of SIMU. To boost convergence speed and improve local perception, we introduce a linear unit that works with the Hopfield unit simultaneously. The intuition unit consists of a linear unit and intuitively map the features in the feature space of penultimate layers to the space of classifications. The memory unit built with Hopfield layer storages the global patterns to identify various human activities. The memory unit can improve global perception, and the linear unit can speedup the convergence. Actually, the input features of a classifier in a deep learning architecture named $\mathcal{P}\left(\mathcal{P}=(f_1\circ\cdots\circ f_N)(\mathcal{X})\right)$, where the model has N stages) need a deep backbone model to extract complex high-dimensional features. We use self-adaptive weights to fusion the prediction result of the two units $h_i(\mathcal{P})$ and $h_m(\mathcal{P})$. The gradient forwarding can automatically tune the weight W_h of each unit. In the training mode, the output of SIMU is weighted fusion of two branches. However, in the evaluating mode, SIMU selects the branch with larger weight. Using the weighted output can ensure that gradient descent's direction can be influenced by intuitive perception and memory patterns. As the result of training, the branch with a larger weight has better classification accuracy in SIMU.

Memory unit stores abundant activity patterns. The teacher model can accumulate richer memories than the student model because of its more sensitive feature perception. After stage distillation, the student model may gain a fuzzy and fundamental perception of human activities with a shared memory unit. SIMU shares memories including

 W_q , W_k , W_v , and W_h with the students' models after the last distilling stage. The SIMU stores the implicit relationship pattern between each features.

Further, logits distilling can warm up and activate the entire model rapidly. The shared memories and soft targets bridge the gap between representation and storage in knowledge distillation. Distilling memories can help the student models approximate their teacher models in few epochs and improve the stability of the whole model.

3.4 Logits distillation

Hinton et al. [27] transfer the generalization ability from a cumbersome model to a smaller model. Vanilla KD distills the soft target, the class probability, predicted by the teacher model to the smaller model. The process of distillation is similar to that of human learning. Teachers provide students with more domain-specific knowledge to solve practical problems. The soft target contains more information than raw one-hot labels because of the hidden relations between classes. The classes are not independent of each other. The soft targets can explain more ignored hidden similarities between classes explained by the teacher model. In the vanilla class probability distillation, the output class logits are $\hat{\mathcal{Y}}_T$, and its corresponding probabilities are $P(\hat{\mathcal{Y}}_T)_c$. For a class logits $\hat{\mathcal{Y}}$, we calculate the probability $P(\hat{\mathcal{Y}})_c$ by using softmax method σ displayed in Equation 8:

$$P(\hat{\mathcal{Y}})_c = \sigma(\hat{\mathcal{Y}}) = \frac{\hat{y}_c}{\sum_{i=1}^C e^{\hat{y}_i}}, \quad c \in \{1, \dots, C\}.$$
 (8)

The vanilla class probability distillation uses both the soft target provided by the cumbersome teacher model and the manually labeled hard target. When distilling the soft target to the student model, the training loss \mathcal{L}_{KD} is combined with the cross-entropy between predicted logits $\hat{\mathcal{Y}}_S$ and soft target $\hat{\mathcal{Y}}_T$ as well as the cross-entropy between predicted logits $\hat{\mathcal{Y}}_S$ and hard ground-truth one-hot label \mathcal{Y} . The Equation 9 displays the combined loss \mathcal{L}_H of the vanilla class probability distillation:

$$\mathcal{L}_{H}(\hat{\mathcal{Y}}_{S}, \hat{\mathcal{Y}}_{T}, \mathcal{Y}) = -\left(\sum_{i=1}^{C} \mathcal{Y}_{i} \log(P(\hat{\mathcal{Y}}_{S})_{i})\right) + \lambda \sum_{i=1}^{C} P(\frac{\hat{\mathcal{Y}}_{T}}{\tau})_{i} \log(P(\frac{\hat{\mathcal{Y}}_{S}}{\tau})_{i}),$$
(9)

where the temperature τ is a relaxation ratio to control the soft targets' smoothing strength. The parameter λ is the weight to control the balance between the influence of the hard label and the soft target.

Logits distillation ensures learning goals of the student model. The target of a deep HAR model is typically the classification of current human activity. To know the learning goals means that the teacher model should teach the student model to obtain more probability information about different activity classes. Stage distillation is to seek which features to be represented by the model. The teacher model can guide the student models to extract certain features that can express the human activity state better. In stage distillation, the teacher model and the student model both have the same number of stages. The same stages of

the teacher model and corresponding student model have similar output features named anchor features. A student cannot master all the knowledge taught by the teacher at once. Therefore, the student model can acquire knowledge from the teacher model step by step. These three questions inspire us to train our student models in stages instead of distilling knowledge only in a single stage.

The hard one-hot labels are not always ground-truth in the real situation [41]. Manually labeled hard labels may introduce new noise for the HAR tasks. The movement features of the user can include many patterns of activity. For example, when running upstairs, the user's activity state should be a combination of several simple activities, including jumping, running, or sometimes walking. The one-hot method to express the actual activity possibility value may ignore some fundamental activities. When the state is labeled as "going upstairs", other related activities such as "walking" or "running" should also gain certain possibilities. However, one-hot labeled logits cannot express those relatively secondary activity classes. Those activity classes are not independent of each other. Therefore, a harder label may have a more significant possibility to train over-fitted activity recognizing models [62].

The soft targets provided by the teacher model reveal the correlation between the implicit inter-class correlations. However, the teacher model can not always provide the right prediction on the possible human activity class. So we use a conditional control technique $Q(\cdot)$ to assume that the manually labeled class can guide the student model [42], and the c-th element of controlled probability provided by the teacher model is $Q(\hat{\mathcal{Y}}_T)_{c}$,

$$R(\hat{\mathcal{Y}}_T)_c = \begin{cases} \gamma, & c = \operatorname{argmax} \mathcal{Y} \text{ and } c \neq \operatorname{argmax} \hat{\mathcal{Y}}_T \\ P(\hat{\mathcal{Y}}_T)_c, & \text{otherwise} \end{cases}$$

$$Q(\hat{\mathcal{Y}}_T) = \sigma(R(\hat{\mathcal{Y}}_T)), \tag{10}$$

where γ is the hardness factor of $R(\cdot)$, and the controlled probability $Q(\hat{\mathcal{Y}}_T)$ corrects the effects of wrong labeled class and smooths the probability distribution of soft targets. Finally, we use $\mathcal{L}_D(\cdot)$ as the loss function to train the frontend classifier of the student model after training previous stages,

$$\mathcal{L}_{D}(\hat{\mathcal{Y}}_{S}, \hat{\mathcal{Y}}_{T}, \mathcal{Y}) = -\left(\sum_{i=1}^{C} \mathcal{Y}_{i} \log(P(\hat{\mathcal{Y}}_{S})_{i})\right) + \lambda \sum_{i=1}^{C} Q(\frac{\hat{\mathcal{Y}}_{T}}{\tau})_{i} \log(P(\frac{\hat{\mathcal{Y}}_{S}}{\tau})_{i}),$$
(11)

After distilling the response logits, SMLDist identifies the target for the student model to learn, and forms a closed loop of learning between models. The whole process of training a slim HAR model by SMLDist is described in Algorithm 1. We improve the ability to extract features for each stage of the student model and guide the student model's classifier strictly by SMLDist.

4 EXPERIMENTAL EVALUATION

We evaluate and analyze SMLDist using various extensive experiments on public HAR datasets. In this section, we will

describe the experiments and the numerical results in the following sections.

4.1 Experimental Setup

We conduct performance evaluation on seven HAR datasets, including RealWorld-HAR [9], MHEALTH [4], [5], HAPT [63], HTC-TMD [6], UCI-HAR [64], DSADS [65], [66], [67], REALDISP [68], [69]. Those datasets are all collected through embedded devices or wearable devices on various positions of users. We will also conduct certain specific analyses on specific datasets. The overall information of those 7 datasets is displayed in Table 1.

RealWorld-HAR dataset² covers 8 sensors, including acceleration, GNSS, gyroscope, light, magnetic field, and sound level data collected on different body positions, including chest, forearm, head, shin, thigh, upper arm, and waist. However, we only select acceleration, gyroscope, and magnetic field to evaluate SMLDist. RealWorld-HAR collects 8 types of activities including climbing stairs down and up, jumping, lying, standing, sitting, running/jogging, and walking from 15 projects (age 31.9 ± 12.4 years old, height 173.1 ± 6.9 cm, weight 74.1 ± 13.8 kg, 8 males and 7 females). In this paper, the training set consists of 13 subjects (age 39.0 ± 23.0 years old, height 173.0 ± 10.0 cm, weight 74.5 ± 20.5 kg, 7 males and 6 females) and the validation set consists of 2 projects (age 26 and 30, height 183cm and 165cm, weight 78kg and 66kg, 1 male and 1 female). The maximum sample rate of raw sensor signals is 49.95Hz, and the final sample rate of aligned sensor signals is 45Hz. We use 5 seconds as the sample window size when preprocessing the RealWorld-HAR dataset's sensor signals. RealWorld-HAR builds a complete dataset of motion and position with abundant subjects and environments in realworld conditions.

MHEALTH dataset³ comprises 12 activities collected from 10 subjects, including standing still, sitting and relaxing, lying down, walking, climbing stairs, waist bends forward, the frontal elevation of arms, knees bending (crouching), cycling, jogging, running, as well as jump front & back. Wearable sensors placed on the subject's right wrist and left ankle provide acceleration values, gyroscope, magnetic field. And sensors placed on the chest provide the subject's electrocardiogram signal value. We only choose acceleration, gyroscope, and magnetic field values to identify subjects' activities for a better evaluation. The sample rate of raw sensor signals is 50Hz, and the window size of each sample is 5 seconds. MHEALTH is a dataset to apply human activity recognition in the domain of health care.

HAPT dataset⁴ consists of 3 static postures (standing, sitting, lying), 3 dynamic postures (walking, walking downstairs, and walking upstairs), and 6 postural transitions (stand-to-sit, sit-to-stand, sit-to-lie, lie-to-sit, stand-to-lie, and lie-to-stand), a total of 12 activities. All the sensor signals (acceleration and gyroscope) are collected from 30 volunteers (age 19-48 years) wearing a smartphone (Samsung Galaxy S II) on their waist. The sample rate of raw

sensor signals is 50Hz, and we randomly divide the dataset into a training set (70% of volunteers) and a validation set (other 30% of volunteers). It's harder to classify the transition classes for HAR models than its elder version, UCI-HAR dataset.

*UCI-HAR dataset*⁵ only consists of 6 basic activities (standing, sitting, lying, walking, walking downstairs, and walking upstairs). Similarly, the sample rate of sensor signals is also 50Hz. Nevertheless, the window size of each sample is 2.56 seconds.

HTC-TMD dataset implements a data collection Android application for 274 participants to divide their transportation status into 10 modes with many real-time samples. The 10 modes include still (107 hours), walking (121 hours), running (61 hours), bike (78 hours), motorcycle (134 hours), car (209 hours), bus (69 hours), metro (95 hours), train (67 hours), and high-speed railway (91 hours). All the participants cover different genders (60% male and 40% female), builds, and ages (20 to 63 years old). In this paper, we selected 70% of samples randomly in the dataset as the training samples and other 30% of samples as the validating samples.

DSADS dataset⁶ contains sensor signals of 19 activities performed by 8 subjects (4 female, 4 male, between the ages 20 and 30). The subjects perform the activities in their style. So there are inter-subject variations in the speeds and amplitudes of some activities between data collected from different subjects. The sample rate of sensor signals is 25Hz, and each sample is segmented to 5 seconds. In this paper, we select samples of 2 subjects randomly as validating set.

REALDISP dataset⁷ collects sensor signals including acceleration, gyroscope, magnetic and quaternion values on realistic displacements (right lower arm, right upper arm, back, left upper arm, left lower arm, right calf, right thigh, left thigh, and left calf). The dataset includes a wide range of physical activities and participants (17 subjects). The 33 dynamic activities in the dataset are more nuanced than other datasets in various positions. The dataset builds on the concepts of ideal placement, self placement, and induced displacement. In the scenario of ideal placement, sensors are displaced strictly on ideal positions by the instructors. The training set consists of all samples of ideal displacement. Self-displacement introduces the error caused by subjective cognition of the participants without explicit instruction. And induced-displacement introduces the error caused by intentional mispositioning of sensors by instructors. We use samples of the other two scenarios as the evaluating set. The REALDISP dataset emphasizes robustness for HAR models due to the error of wearing position in reality. So models with better robustness can have better performance evaluated using REALDISP dataset.

The benchmark based on seven datasets can evaluate HAR models about their universality, robustness, and compatibility. Sensor values can fluctuate abnormally as outliers due to system errors in the embedded devices.

^{2.} https://sensor.informatik.uni-mannheim.de/index.html#dataset_realworld

^{3.} https://archive.ics.uci.edu/ml/datasets/MHEALTH+Dataset

^{4.} https://archive.ics.uci.edu/ml/datasets/Smartphone-Based+Recognition+of+Human+Activities+and+Postural+Transitions

^{5.} https://archive.ics.uci.edu/ml/datasets/Human+Activity+Recognition+Using+Smartphones

^{6.} https://archive.ics.uci.edu/ml/datasets/Daily+and+Sports+Activities

^{7.} https://archive.ics.uci.edu/ml/datasets/REALDISP+Activity+Recognition+Dataset

TABLE 1
Description of seven public human activity recognition datasets.

Name	Subjects	Activities	Body positions	Sensors	Sample Rate	Window size
RealWorld-HAR	15	8	7	3	45Hz	5 seconds
UCI-HAR	30	6	2	2	50Hz	2.56 seconds
HTC-TMD	224	10	3	3	47Hz	5 seconds
MHEALTH	10	12	2	2	50Hz	5 seconds
HAPT	30	12	1	2	50Hz	3 seconds
DSADS	8	19	5	3	50Hz	5 seconds
REALDISP	17	33	9	3	50Hz	3 seconds

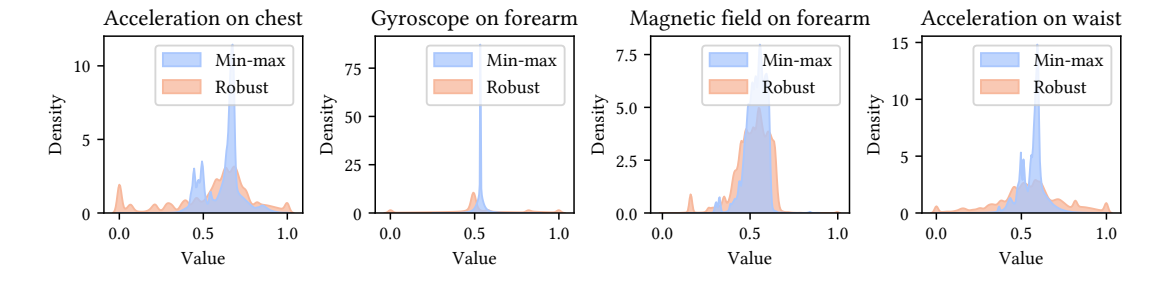


Fig. 3. Kernel distribution estimation of sensor samples in RealWorld-HAR dataset processed by minimum-maximum scaling and robust scaling.

These outliers can make the numerical distribution in the normal range very dense to be distinguished by the model. When normalizing the raw sensor data by the minimum-maximum scaling method displayed in Equation 12, normal values are clustered too densely in a range rather than distributed relatively evenly throughout the numerical distribution.

$$S_{minmax}(\mathcal{X}) = \frac{\text{clip}(\mathcal{X}, \min(\mathcal{X}), \max(\mathcal{X}))}{\max(\mathcal{X}) - \min(\mathcal{X})}.$$
 (12)

We use the robust scaling method displayed in Equation 13 to avoid the significant noise introduced by the absolute boundary of raw sensor data.

$$IQR(\mathcal{X}) = Q_{3}(\mathcal{X}) - Q_{1}(\mathcal{X})$$

$$L_{lower}(\mathcal{X}) = Q_{1}(\mathcal{X}) - 1.5 \cdot IQR(\mathcal{X})$$

$$L_{upper}(\mathcal{X}) = Q_{3}(\mathcal{X}) + 1.5 \cdot IQR(\mathcal{X})$$

$$S_{robust}(\mathcal{X}) = \frac{\text{clip}(\mathcal{X}, L_{lower}(\mathcal{X}), L_{upper}(\mathcal{X}))}{4 \cdot IQR(\mathcal{X})},$$
(13)

where Q_1 is the first quartile of raw sensor value \mathcal{X} , Q_3 is the third quartile of raw sensor value \mathcal{X} , and IQR is the inter-quartile range of raw sensor value \mathcal{X} . As displayed in Figure 3, we evaluate the distributions of samples normalized by the minimum-maximum scaling and the robust scaling RealWorld-HAR dataset. We use the modules of each sensor vectors to display distributions. Ignoring the effects of extreme maximum-minimum scaled normalization can result in an overly dense distribution of the results. An overly dense distribution may increase the difficulty of the model sensing input feature samples. We use robust scaling to process sensor data in experiments mentioned in the following sections. We set each batch's size of training and validating samples to 256, the learning rate to 1×10^{-4} , and use the Ranger [70] algorithm to optimize the model. We use Python to build all the modeling and evaluating

TABLE 2 Evaluation environments of SMLDist.

Туре	Information									
Server	Model Untel Xeon Gold 6230 Model NVIDIA Tesla V100S Operating system CentOS Linux 7.4.1708	Frequency 2.10GHz 187Gil Performance Memor 130TFLOPS 32GiB Architecture amd64								
Embedded device	Model NVIDIA Carmel Model NVIDIA Volta Operating system Ubuntu 18.04.5 LTS	Frequency 2.30GHz Performance 11TFLOPS Architec aarch								

code and implement the models based on PyTorch [48] 1.7.1. We perform all modeling and most performance evaluation experiments in this section on a server cluster node with NVIDIA TESLA V100S GPU and Intel Xeon Gold 6230 CPU. Also, we perform experiments of embedded platforms on an NVIDIA Jetson AGX Xavier with NVIDIA Carmel ARM v8.2 64-Bit CPU and NVIDIA Volta GPU (with 512 NVIDIA CUDA cores and 64 Tensor cores). In particular, both CPU and GPU share the same memory of 32GB in NVIDIA Jetson AGX Xavier.

4.2 Evaluation of Compression Ratio

We perform a series of quantitative analysis on SMLDist and a series of evaluations of compression performance. We analyze the effect of SMLDist from different perspectives, including the effect of stage distilling, evaluation of soft targets, and compression performance using SMLDist.

Firstly, we evaluate the performance, including accuracy and F1 macro score of student models with different compression ratios. We use the same configurations of the

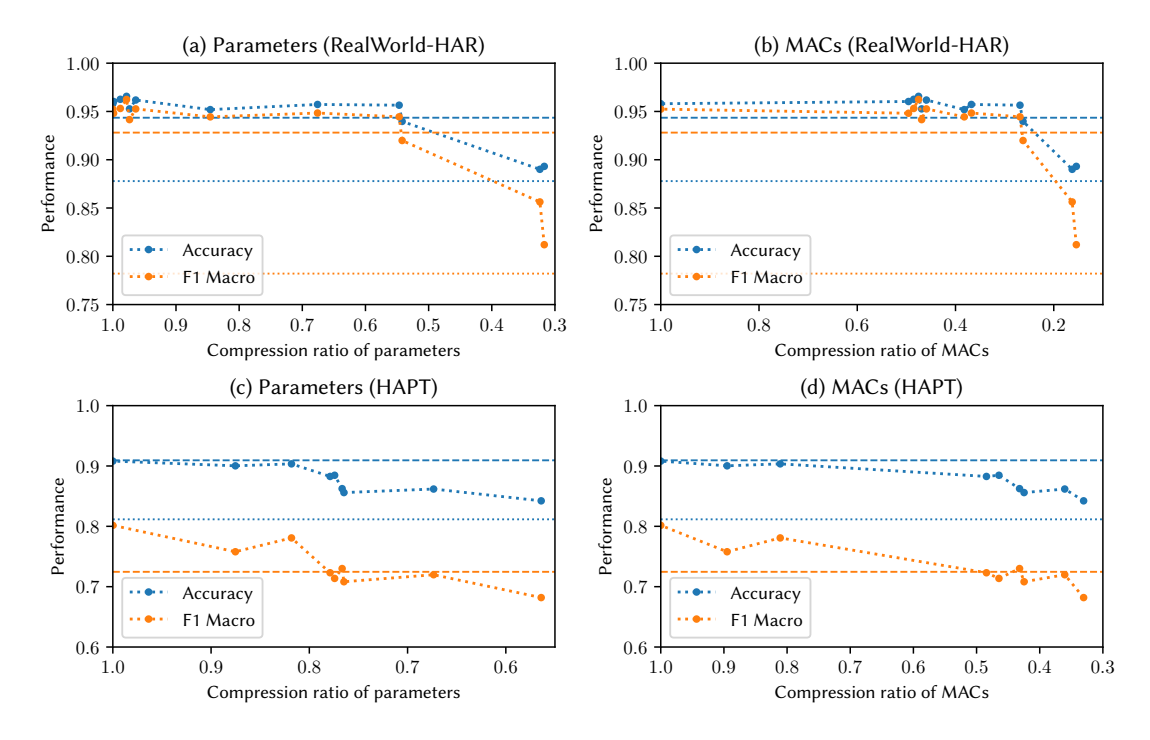


Fig. 4. Performance curve of student models with decreasing compression ratio.

teacher models to compress the student models. We use RealWorld-HAR dataset and HAPT dataset to evaluate the performance variation caused by the parameters' compression and multiply accumulates (MACs). With the compression of the spatial and temporal overhead, we find that the student models' performance decrease is small and in a reasonable range, as displayed in Figure 4. We annotate the performance of the common teacher model as the horizontal dashed line in the Figure 4. On the RealWorld-HAR dataset, the self-distilled model and models with a higher compression ratio have better performance than the original teacher model on accuracy and F1 macro score. The F1 macro score on the HAPT dataset of the self-distilled model and models with larger compression ratios are higher than the F1 macro score of the teacher model. The smallest student model's performance trained without SMLDist on those 2 datasets is listed as the figure's horizontal dotted line. The student models with the highest compression ratio on 2 datasets both get apparent improvement than the model trained independently with the same configurations. Also, using SMLDist as the self-distilling technique can improve the performance of the trained model.

4.3 Evaluation of SIMU

We evaluate the weights and output logits of the SIMU in the best teacher model and its student on the RealWorld dataset. Figure 5 displays these results. The validation sets used to evaluate SIMU consist of continuous activities collected on 2 subjects (samples from #0 to #559 are collected on subject #14 in the RealWorld dataset. Other samples are collected on subject #15 in the RealWorld dataset). All the samples collected on the same subject are temporally continuous.

The self-adaptive weight of the memory branch increases while the weight of the intuition branch decreases. Figure 5(a) displays the memory branch's softmaxed self-adaptive weights and the intuition branch when training the teacher model. The dashed vertical line annotates the epoch in which the model has the best performance. We use this best model to distilling knowledge to the student model. Figure 5(b) displays the memory branch's softmaxed self-adaptive weights and the intuition branch when training the student model. The memory branch's weight decreases continuously when training the teacher model and the student model, which means the intuition branch's importance decreases as stored information in the memory branch increases under this condition.

The intuition branch leads the memory branch to learn. Figure 5(c) displays all samples' softmaxed output logits in the student model's memory branch's validation set. Figure 5(d) displays corresponding logits from the student model's intuition branch. Comparing 5(c) with 5(d), the memory branch can predict a well-trained model than the intuition branch better. Figure 5(e) displays the fused logits processed by softmax of all samples in the validation set from the memory branch and the student model's intuition branch. Figure 5(f) displays the ground-truth of activity in validation set. The training process uses the fused logits as the model's output, which is affected by the intuition branch and the memory branch in common. However, the cooperating training process helps the memory branch gain a better performance. In Table 3, M means using a memory branch as a classifier independently when training and predicting, and I means using an intuition branch independently which is equal to the vanilla MobileNet V3 model. I+M is the weighted fusion of the memory branch and the intuition branch. Compared with the result of SIMU, we can know

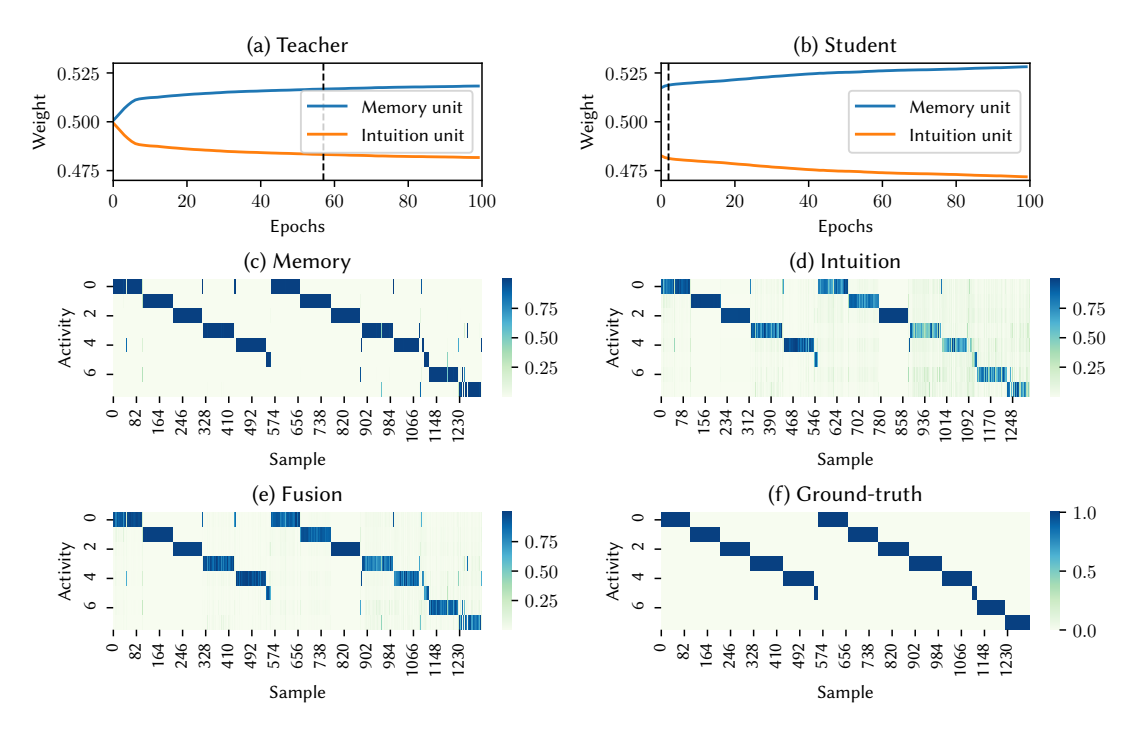


Fig. 5. Evaluation of weights and logits in SIMU of best model trained on RealWorld-HAR dataset.

TABLE 3 Ablation evaluation of SIMU.

Dataset	Metric	M	I	I+M	SIMU
RealWorld-HAR	Accuracy (%)	84.43	89.16	95.65	95.73
	F1 Macro (%)	77.37	85.14	94.73	94.84
UCI-HAR	Accuracy (%)	95.75	95.07	95.79	96.00
	F1 Macro (%)	95.69	94.94	95.68	95.88
HTC-TMD	Accuracy (%)	92.98	92.85	93.10	93.18
	F1 Macro (%)	92.71	92.56	92.76	92.87
MHEALTH	Accuracy (%)	98.96	98.31	99.12	99.41
	F1 Macro (%)	98.63	98.43	99.11	99.38
HAPT	Accuracy (%)	88.18	90.58	90.65	92.11
	F1 Macro (%)	72.89	72.79	74.85	84.28
DSADS	Accuracy (%)	80.70	84.07	97.54	97.72
	F1 Macro (%)	77.24	81.55	97.55	97.66
REALDISP	Accuracy (%)	91.40	92.72	93.49	94.00
	F1 Macro (%)	92.11	92.17	93.19	93.79

that the intuition branch can assist the memory branch to get better performance in training process. The optimizer can automatically improve the weight of the branch with larger reliability.

4.4 Performance Evaluation

We conduct series of experiments to evaluate the performance of SMLDist. The performance comparison of classification among various state-of-the-art methods and the model produced by SMLDist is displaced in Table 4. The models produced by SMLDist are based on a backbone of MobileNet V3 [24]. Both performance and efficiency are evaluation indicators of different methods. The goal

of SMLDist is to find a balance between efficiency and performance.

In Table 4, we perform the experiments on the 7 public datasets mentioned above to compare the vanilla MobileNet V3 models built by SMLDist with other well-designed architectures. As the table displayed, the models produced by SMLDist achieve a better performance of accuracy and F1 macro score than other baseline methods. The calculation of F1 macro score is defined as

$$\begin{aligned} \text{Precision} &= \frac{\text{TP}}{\text{TP} + \text{FP}} \\ \text{Recall} &= \frac{\text{TP}}{\text{TP} + \text{FN}} \\ \text{F1} &= 2 \cdot \frac{\text{Precision} \cdot \text{Recall}}{\text{Precision} + \text{Recall}} \end{aligned} \tag{14}$$

where TP is true positives, FP is false positives, and FN is false negatives.

We also evaluate the scale of parameters and multiply accumulates (MACs), representing the model's storage overhead and computational overhead of deep learning operations.

The models produced by SMLDist achieve better performance than other methods with reasonable overhead. GlobalFusion has a smaller scale of parameters and MACs. However, in more demanding conditions, it has more latent capacity to improve robustness. For example, transitions between activities are hard to recognize, and the error in transitions may cause a sharp drop in the F1 macro score. As displayed in Table 1, samples in RealWorld-HAR dataset have the most channels of sensors.

A growing number of sensors may cause an increase in the computational and spatial overhead of the HAR model. The balance between efficiency and performance

TABLE 4
Predicting performance and energy & time cost comparison on 7 public datasets.

Method	Dataset	Accuracy (%)	F1 Macro (%)	MACs (M)	Parameters (M)	Time cost (ms/sample)	Energy cost $(mW \cdot h/\text{sample})$	Energy cost $(W \cdot h/\text{day})$
	RealWorld-HAR UCI-HAR	76.72 90.77	66.34 90.80	14.3203 10.4268	0.4144 1.9041	14.479 2.816	0.0288 0.0055	0.4978 0.1873
DeepConv- LSTM [11]	HTC-TMD	78.54	77.95	11.4250	0.3293	4.344	0.0033	0.1839
100								
ďď	MHEALTH	91.69	91.50	13.4253	0.3530	4.091	0.0104	0.1793
) S	HAPT	84.55	70.71	7.3044	0.1955	2.861	0.0070	0.2024
п –	DSADS	65.83	65.89	8.0150	0.8862	3.509	0.0072	0.1248
	REALDISP	84.61	83.14	14.5689	1.5883	13.341	0.0935	2.6933
	RealWorld-HAR	90.61	89.95	189.3646	12.3379	12.525	0.0243	0.4194
se	UCI-HAR	94.29	94.10	12.8616	2.5653	11.028	0.0193	0.6529
AttnSense [14]	HTC-TMD	91.45	90.98	10.5904	2.0591	23.318	0.0469	0.8102
nS [14	MHEALTH	98.60	98.70	72.9328	5.0763	43.218	0.0865	1.4951
#	HAPT	87.61	74.84	12.6488	0.9057	10.455	0.0203	0.5855
4	DSADS	80.61	80.62	192.6510	3.8641	85.395	0.1437	2.4838
	REALDISP	88.35	87.36	430.0884	12.3149	88.268	0.1559	4.4890
	RealWorld-HAR	90.15	83.58	75.8809	69.4538	19.870	0.0535	0.9242
SparseSense [15]	UCI-HAR	92.56	92.51	14.4920	13.3184	4.411	0.0105	0.3538
_ še.	HTC-TMD	87.09	86.52	10.9658	10.0449	4.142	0.0101	0.1742
seS ₍	MHEALTH	98.75	98.73	25.4207	23.2567	43.218	0.0865	1.4951
ar _	HAPT	86.25	77.04	7.3247	6.7329	10.455	0.0203	0.5855
Şς	DSADS	73.73	70.61	53.9532	49.5548	13.114	0.0343	0.5932
	REALDISP	89.23	88.01	194.2680	89.1294	19.721	0.1005	2.8939
	RealWorld-HAR	83.66	53.50	2102.7232	2100.6331	-	-	-
	UCI-HAR	94.29	94.09	22.2980	22.0839	40.312	0.2892	9.7604
Z [2	HTC-TMD	90.71	90.45	46.3340	46.0250	42.563	0.2362	4.0818
IndRNN [19], [20]	MHEALTH	98.53	98.53	336.7826	335.9470	161.545	1.3769	23.7928
pd [61	HAPT	82.46	58.81	111.1662	110.6870	62.914	0.2079	5.9886
4 -	DSADS	74.17	73.90	888.1407	443.1107	233.728	1.8976	32.7912
	REALDISP	-	-	1501.8984	1500.1324	-	-	-
	RealWorld-HAR	83.59	78.86	704.8512	566.6437	45.519	0.2248	3.8852
ŧ	UCI-HAR	94.53	94.52	73.3457	59.5125	6.854	0.0270	0.9115
Ž ≅	HTC-TMD	87.05	86.47	108.6073	87.6933	9.013	0.0393	0.6795
EmbraceNet [17], [18]	MHEALTH	98.60	98.69	264.0113	212.4775	17.291	0.0822	1.4201
. 7 br	HAPT	88.72	77.77	44.4001	36.1818	5.241	0.0022	0.5678
<u>[</u> g =	DSADS	74.78	73.04	517.4861	208.8154	21.272	0.0883	1.5252
щ	REALDISP	87.71	86.40	569.8615	458.9135	38.641	0.1773	5.1073
		94.12			1.5519	29.726	0.1454	
ᄄ	RealWorld-HAR UCI-HAR	94.12 95.86	93.44 95.82	148.2688 158.3610	1.5519	29.726 8.449	0.1454	2.5121 0.9585
.00								
بالة 2) يا	HTC-TMD	91.92	91.46	27.3844	0.6172	9.047	0.0315	0.5447
alFt [16]	MHEALTH	98.60	98.32	42.7075	0.7704	11.363	0.0383	0.6619
GlobalFusion [16]	HAPT	85.40	56.59	23.3884	0.6106	29.011	0.0720	2.0728
\Box	DSADS	82.59	82.17	741.0103	28.7801	19.035	0.0744	1.2852
	REALDISP	91.25	89.90	1531.4923	54.6268	23.677	0.1100	3.1667
	RealWorld-HAR	95.73	94.84	96.5486	19.1775	13.282	0.0339	0.9768
st	UCI-HAR	96.00	95.88	34.0904	9.2028	8.653	0.0209	0.6013
Ď.	HTC-TMD	93.18	92.87	71.5737	3.3807	11.090	0.0240	0.4139
1	MHEALTH	99.41	99.38	85.2107	3.7107	13.727	0.0287	0.4966
SMLDist	HAPT	92.11	84.28	51.8479	3.7800	14.626	0.0302	0.8692
-,	DSADS	97.72	97.66	320.0500	18.5336	13.684	0.0385	0.6654
	REALDISP	94.00	93.79	233.2098	20.3682	11.582	0.0341	0.9827

is essential to improve the robustness of the HAR model. The method based on recurrent layers, such as IndRNN, needs more parameters and more computation resources to apply recurrent operations. In the RealWorld-HAR dataset, IndRNN's parameters reach 2100.6331 million, and MACs reach 2102.7232 million. Other methods that combine the convolutional operations and recurrent operations enable the recurrent layers to focus more on perceiving temporal patterns instead of extracting lots of redundant features. AttnSense, IndRNN, and GlobalFusion need an extra process of FFT to extract spectral features. Those models combined with recurrent operations and convolutional operations usu-

ally design submodels for each position's sensor in their architecture. This strategy is usable but improves the computational overhead dramatically. GlobalFusion has good performance and small computational overhead on most datasets. But its parameters reach 1531.4923 million and its MACs reach 1500.1324 million on the REALDISP dataset. Because the model trained on REALDISP is too huge, we cannot train the IndRNN model on the training server deployed with NVIDIA TESLA V100S GPU. So we cannot evaluate the accuracy and F1 macro score performance on REALDISP dataset, which means it is hard to deploy an IndRNN model in an embedded device. However, we use

TABLE 5
Predicting performance comparison with equal compression ratio on 7 public datasets.

Method	Accuracy (%) ≈							F1 Macro (%)						
	RealWorld-HAR	UCL HAR	HTC- TMD	MHEALTH	HAPT	DSADS	REALDISP	RealWorld-HAR	UC_LHA_R	HTC- TMD	MHEALTH	HAPT	DSADS	REALDISP
Raw	82.52	94.64	94.45	97.87	84.15	95.53	93.00	82.27	94.58	94.24	98.00	42.13	95.51	92.86
Vanilla KD [27] CKD [42] FitNets [28] NST [52] FNKD [41] SPKD [71] FT [54]	90.31 93.21 90.08 92.37 86.56 86.18 84.27	94.70 95.08 95.52 94.94 94.94 95.15 95.76	92.95 92.41 88.53 86.13 92.11 92.40 92.15	98.09 97.65 98.90 98.23 96.25 92.13 94.11	85.15 91.12 86.98 84.38 87.90 86.14 86.75	93.86 96.05 95.26 95.88 96.93 94.65 95.00	91.69 93.48 91.85 92.83 92.84 93.20 92.46	86.09 89.29 84.14 89.10 80.86 69.78 68.87	94.67 95.03 95.46 94.89 94.83 95.11 95.70	92.70 92.08 81.50 79.37 91.72 92.02 91.79	98.11 97.78 98.97 97.55 96.34 90.53 93.92	43.92 71.49 43.75 44.32 56.27 45.05 44.92	93.27 95.84 95.17 95.76 96.86 94.63 94.91	93.12 93.22 91.37 91.95 92.56 92.67 91.86
SMLDist	95.73	96.00	93.18	99.41	92.11	97.72	94.00	94.84	95.88	92.87	99.38	84.28	97.66	93.79

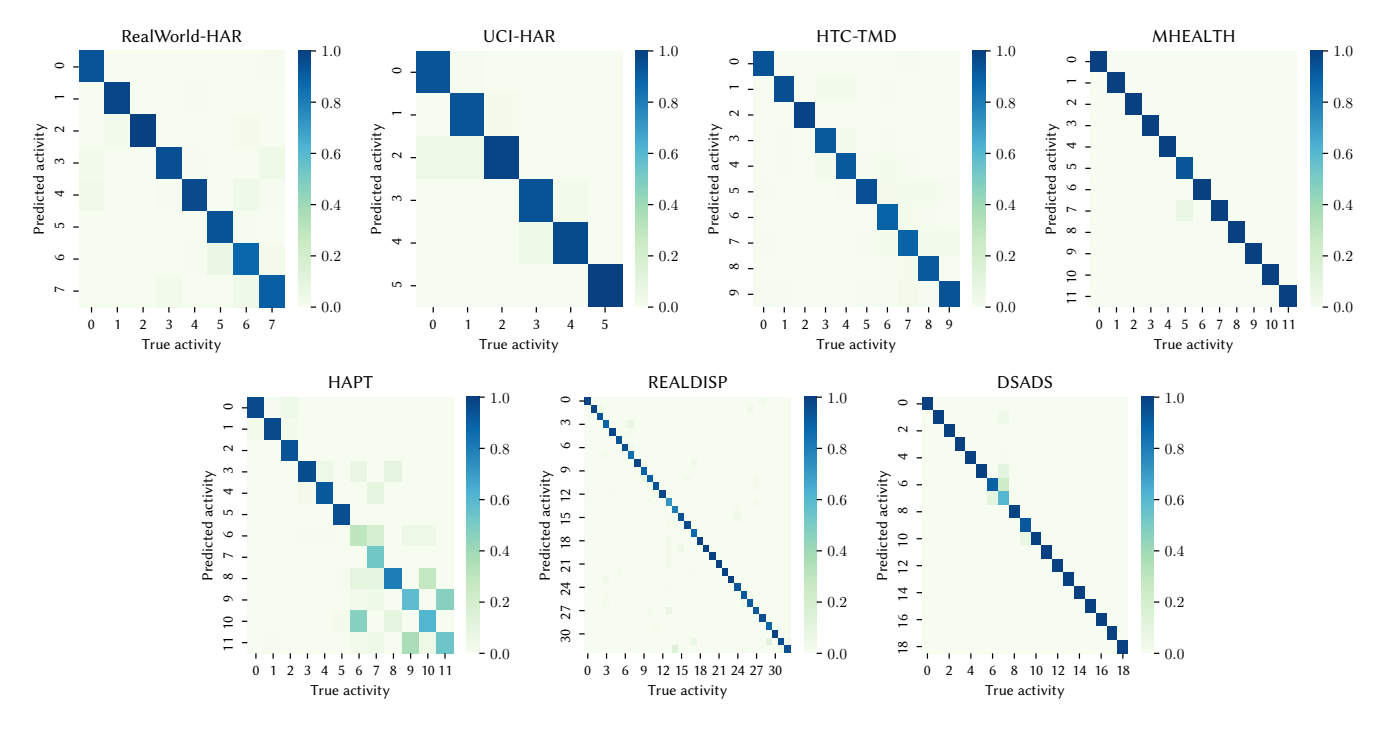


Fig. 6. Confusion matrix on public datasets.

MobileNet V3 as the backbone structure to produce the evaluation of SMLDist, which is constructed by convolutional operations completely. The evaluated models can get better accuracy than other models, and the increase of sensors would not cause an apparent increase in computational overheads. As a modeling pipeline based on knowledge distillation, SMLDist can also be used to build HAR models based on other backbone architectures.

To examine the energy and time overhead of the models produced by SMLDist, we deploy the models into an NVIDIA Jetson AGX Xavier and use them to predict on validating sets of all seven public datasets. We measure the actual energy cost of the embedded device when the device is free. Moreover, we measure the energy cost and executing time when predicting on the whole validating set of those public datasets. The difference between the

predicting energy cost and the free energy cost is the real energy cost consumed by the model. As displayed in Table 4, the longest consumed time per sample when predicting with the sensor configured like the REALDISP dataset is 11.582 milliseconds. Because the REALDISP dataset captures 9 IMU sensors' positions, there are more channels of sensor signals fed into the model. So the model configured on the REALDISP dataset consumes more energy than other models. Because IndRNN models are too huge, we cannot deploy models trained on REALDISP dataset and RealWorld-HAR dataset on the embedded device to evaluate energy and time cost. As evaluated in the above experiments, the evaluated models produced by SMLDist can be deployed into an embedded device with reasonable energy and time cost. The evaluated models cost less than 2 $W \cdot h/\text{day}$ on all evaluated datasets, which has better

performance and efficiency than other models.

As displayed in Figure 6, we find that transition classes in HAPT datasets are fewer than other classes of single activities. Also, in the large transportation mode dataset of HTC, we find ambiguity among motorcycle and bike modes. Motorcycle mode also has ambiguity with car mode. Bus mode is more challenging to be recognize than other modes. In REALDISP dataset, the raw sensor values are continuous, and walking samples are far more than samples of other activities. The quantitative imbalance among different activities increases the difficulty of classification. The F1 macro score displayed in Table 4 exclaims that the evaluated models provided by SMLDist have better classification robustness than other state-of-the-art models.

Different KD pipelines have different performances on HAR problems. We evaluate various knowledge distilling pipelines with state-of-the-art in Table 5. To compare the performance of different KD pipelines, we ensure all the teacher models and the student models in different KD pipelines have the environmental configuration (structure, compression ratio, and dataset). We evaluate the raw mode of training the student model. In the raw mode, we train the student model independently. The student models trained by KD pipelines have better performance than the raw student model under most of the conditions. The experiments display that SMLDist has better robustness when compressing the deep models. The performances of student models powered by SMLDist usually have less loss than models trained by other KD pipelines. Under some more demanding conditions, Models compressed by other KD pipelines dramatically influence the F1 macro score of the predictions. As the most classical baseline of KD methods, vanilla KD improves the performance of the lightweight student model better than the independently trained model with equal computational overheads on most of the datasets. However, the effects of vanilla KD have a significant loss on HTC-TMD, DSADS, and REALDISP. Part of mispredicted soft targets may mislead the student model and have adverse effects. CKD enhances the quality of distilled soft targets by mapping the wrong soft targets to the hard labels. So the CKD has a considerable improvement on most of the datasets. Feature normalization of KD (FNKD) may not always has a positive effect. On a larger-scaled dataset, such as RealWorld-HAR and HTC-TMD, the student models trained by FNKD have a slight decrease in performance compared with the models trained by vanilla KD. As displayed in Table 5, SMLDist is more robust in the HAR tasks under more conditions. Both the representation of the model and the efficiency of distillation have reasonable improvements.

5 CONCLUSION AND FUTURE WORK

This paper describes the framework of SMLDist, a structural distilling pipeline. SMLDist builds a multi-level pipeline of knowledge distillation with the combination of stage distillation, memory distillation, and logits distillation. The knowledge of a deep neural model has multiple schemas. A model builds instant knowledge in the classification task, such as the intermediate features and the predicted logits, and stored knowledge, such as relationship patterns of high-dimensional features.

Stage distillation constrains the essential representation of the student model to mimic the teacher model. The intermediate features are the most basic information extracted from the raw input data. Constraining the learning direction of those representations can transfer the representation explicitly to the student models. It can also avoid the student models' representation damaging significantly when the computational resources have decreased considerably.

Memory distillation teaches the student models how to react to the high-dimensional features and explain the relationship between those features. The fundamental unit of memory distillation is SIMU, a self-adaptive unit based on Hopfield networks to provide the final layers of a deep neural classifier with better storage ability.

Logits distillation has the most intuitive direction of the probability distribution of the classification labels. We construct the distilled logits by a smoothed conditional rule to keep the probable distribution and improve the correctness of the soft target.

SMLDist is an effective method to build HAR models with better efficiency and less performance loss. SMLDist can boost any deep learning structures based on convolutional layers. Models optimized by SMLDist can work with reasonable energy costs on embedded devices. There are also lots of challenges to solve HAR problems. HAR models could have better compatibility with data collected at different positions of the user's body. The fusion of various positions can improve the performance of HAR. However, it may also improve the energy costs of sensors and the computational models. We will try to design a training schema to build HAR models with better generalization ability to have better robustness on various sensors, environments, and users in the future.

ACKNOWLEDGMENTS

This work was supported in part by the National Key Research and Development Program under Grant 2018YFB0505200, the Action Plan Project of the Beijing University of Posts and Telecommunications supported by the Fundamental Research Funds for the Central Universities under Grant 2019XD-A06, the National Natural Science Foundation of China under Grant 61872046, the Joint Research Fund for Beijing Natural Science Foundation and Haidian Original Innovation under Grant L192004, Beijing Natural Science Foundation under Grant 4212024, the Key Research and Development Project from Hebei Province under Grant 19210404D, the Science and Technology Plan Project of Inner Mongolia Autonomous Region under Grant 2019GG328 and the Open Project of the Beijing Key Laboratory of Mobile Computing and Pervasive Device.

REFERENCES

- [1] T. van Kasteren, G. Englebienne, and B. J. A. Kröse, "An activity monitoring system for elderly care using generative and discriminative models," *Pers. Ubiquitous Comput.*, vol. 14, no. 6, pp. 489–498, 2010. [Online]. Available: https://doi.org/10.1007/s00779-009-0277-9
- [2] Y. Zhu, H. Luo, F. Zhao, and R. Chen, "Indoor/outdoor switching detection using multisensor densenet and lstm," *IEEE Internet of Things Journal*, vol. 8, no. 3, pp. 1544–1556, 2021.

- [3] A. Almeida and A. Alves, *Activity Recognition for Movement-Based Interaction in Mobile Games*. New York, NY, USA: Association for Computing Machinery, 2017. [Online]. Available: https://doi.org/10.1145/3098279.3125443
- [4] O. Baños, R. García, J. A. H. Terriza, M. Damas, H. Pomares, I. R. Ruiz, A. Saez, and C. Villalonga, "mhealthdroid: A novel framework for agile development of mobile health applications," in Ambient Assisted Living and Daily Activities 6th International Work-Conference, IWAAL 2014, Belfast, UK, December 2-5, 2014. Proceedings, ser. Lecture Notes in Computer Science, L. Pecchia, L. L. Chen, C. D. Nugent, and J. Bravo, Eds., vol. 8868. Springer, 2014, pp. 91–98. [Online]. Available: https://doi.org/10.1007/978-3-319-13105-4_14
- [5] L. T. Nguyen, M. Zeng, P. Tague, and J. Zhang, "Recognizing new activities with limited training data," in *Proceedings of the 2015 ACM International Symposium on Wearable Computers*, ISWC 2015, Osaka, Japan, September 7-11, 2015, K. Mase, M. Langheinrich, D. Gatica-Perez, K. V. Laerhoven, and T. Terada, Eds. ACM, 2015, pp. 67–74. [Online]. Available: https://doi.org/10.1145/2802083.2808388
- [6] M. Yu, T. Yu, S. Wang, C. Lin, and E. Y. Chang, "Big data small footprint: The design of A low-power classifier for detecting transportation modes," *Proc. VLDB Endow.*, vol. 7, no. 13, pp. 1429–1440, 2014. [Online]. Available: http://www.vldb.org/pvldb/vol7/p1429-yu.pdf
- [7] Y. Zhu, F. Zhao, and R. Chen, "Applying 1d sensor densenet to sussex-huawei locomotion-transportation recognition challenge," in Adjunct Proceedings of the 2019 ACM International Joint Conference on Pervasive and Ubiquitous Computing and Proceedings of the 2019 ACM International Symposium on Wearable Computers, ser. UbiComp/ISWC '19 Adjunct. New York, NY, USA: Association for Computing Machinery, 2019, p. 873–877. [Online]. Available: https://doi.org/10.1145/3341162.3345571
- [8] Y. Zhu, H. Luo, R. Chen, F. Zhao, and L. Su, "Densenetx and gru for the sussex-huawei locomotion-transportation recognition challenge," in Adjunct Proceedings of the 2020 ACM International Joint Conference on Pervasive and Ubiquitous Computing and Proceedings of the 2020 ACM International Symposium on Wearable Computers, ser. UbiComp-ISWC '20. New York, NY, USA: Association for Computing Machinery, 2020, p. 373–377. [Online]. Available: https://doi.org/10.1145/3410530.3414349
- [9] T. Sztyler and H. Stuckenschmidt, "On-body localization of wearable devices: An investigation of position-aware activity recognition," in 2016 IEEE International Conference on Pervasive Computing and Communications, PerCom 2016, Sydney, Australia, March 14-19, 2016. IEEE Computer Society, 2016, pp. 1–9. [Online]. Available: https://doi.org/10.1109/PERCOM.2016.7456521
- [10] L. Wang, H. Gjoreski, M. Ciliberto, S. Mekki, S. Valentin, and D. Roggen, "Enabling reproducible research in sensor-based transportation mode recognition with the sussex-huawei dataset," *IEEE Access*, vol. 7, pp. 10870–10891, 2019. [Online]. Available: https://doi.org/10.1109/ACCESS.2019.2890793
- [11] F. J. Ordóñez and D. Roggen, "Deep convolutional and lstm recurrent neural networks for multimodal wearable activity recognition," Sensors, vol. 16, no. 1, 2016. [Online]. Available: https://www.mdpi.com/1424-8220/16/1/115
- [12] V. Mnih, N. Heess, A. Graves, and K. Kavukcuoglu, "Recurrent models of visual attention," in Advances in Neural Information Processing Systems 27: Annual Conference on Neural Information Processing Systems 2014, December 8-13 2014, Montreal, Quebec, Canada, Z. Ghahramani, M. Welling, C. Cortes, N. D. Lawrence, and K. Q. Weinberger, Eds., 2014, pp. 2204–2212. [Online]. Available: https://proceedings.neurips.cc/paper/2014/hash/09c6c3783b4a70054da74f2538ed47c6-Abstract.html
- [13] A. Vaswani, N. Shazeer, N. Parmar, J. Uszkoreit, L. Jones, A. N. Gomez, L. Kaiser, and I. Polosukhin, "Attention is all you need," in Advances in Neural Information Processing Systems 30: Annual Conference on Neural Information Processing Systems 2017, December 4-9, 2017, Long Beach, CA, USA, I. Guyon, U. von Luxburg, S. Bengio, H. M. Wallach, R. Fergus, S. V. N. Vishwanathan, and R. Garnett, Eds., 2017, pp. 5998–6008. [Online]. Available: https://proceedings.neurips.cc/paper/2017/hash/3f5ee243547dee91fbd053c1c4a845aa-Abstract.html
- [14] H. Ma, W. Li, X. Zhang, S. Gao, and S. Lu, "Attnsense: Multi-level attention mechanism for multimodal human activity recognition," in Proceedings of the Twenty-Eighth International Joint Conference on Artificial Intelligence, IJCAI 2019, Macao, China, August 10-16, 2019,

- S. Kraus, Ed. ijcai.org, 2019, pp. 3109–3115. [Online]. Available: https://doi.org/10.24963/ijcai.2019/431
- [15] A. Abedin, S. H. Rezatofighi, Q. Shi, and D. C. Ranasinghe, "Sparsesense: Human activity recognition from highly sparse sensor data-streams using set-based neural networks," in Proceedings of the Twenty-Eighth International Joint Conference on Artificial Intelligence, IJCAI-19. International Joint Conferences on Artificial Intelligence Organization, 7 2019, pp. 5780–5786. [Online]. Available: https://doi.org/10.24963/ijcai.2019/801
- [16] S. Liu, S. Yao, J. Li, D. Liu, T. Wang, H. Shao, and T. Abdelzaher, "Globalfusion: A global attentional deep learning framework for multisensor information fusion," *Proc. ACM Interact. Mob. Wearable Ubiquitous Technol.*, vol. 4, no. 1, Mar. 2020. [Online]. Available: https://doi.org/10.1145/3380999
- [17] J. Choi and J. Lee, "Embracenet: A robust deep learning architecture for multimodal classification," *Inf. Fusion*, vol. 51, pp. 259–270, 2019. [Online]. Available: https://doi.org/10.1016/j. inffus.2019.02.010
- [18] J.-H. Choi and J.-S. Lee, "Embracenet for activity: A deep multimodal fusion architecture for activity recognition," in Adjunct Proceedings of the 2019 ACM International Joint Conference on Pervasive and Ubiquitous Computing and Proceedings of the 2019 ACM International Symposium on Wearable Computers, ser. UbiComp/ISWC '19 Adjunct. New York, NY, USA: Association for Computing Machinery, 2019, p. 693–698. [Online]. Available: https://doi.org/10.1145/3341162.3344871
- [19] B. Zhao, S. Li, and Y. Gao, "Indrnn based long-term temporal recognition in the spatial and frequency domain," in Adjunct Proceedings of the 2020 ACM International Joint Conference on Pervasive and Ubiquitous Computing and Proceedings of the 2020 ACM International Symposium on Wearable Computers, ser. UbiComp-ISWC '20. New York, NY, USA: Association for Computing Machinery, 2020, p. 368–372. [Online]. Available: https://doi.org/10.1145/3410530.3414355
- [20] B. Zhao, S. Li, Y. Gao, C. Li, and W. Li, "A framework of combining short-term spatial/frequency feature extraction and long-term indrnn for activity recognition," *Sensors*, vol. 20, no. 23, p. 6984, 2020. [Online]. Available: https://doi.org/10.3390/s20236984
- [21] S. Li, W. Li, C. Cook, C. Zhu, and Y. Gao, "Independently recurrent neural network (indrnn): Building a longer and deeper RNN," in 2018 IEEE Conference on Computer Vision and Pattern Recognition, CVPR 2018, Salt Lake City, UT, USA, June 18-22, 2018. IEEE Computer Society, 2018, pp. 5457–5466. [Online]. Available: http://openaccess.thecvf.com/content_cvpr_2018\html/Li_Independently\\ Recurrent\\ Neural\\ CVPR\\ 2018\\ paper.html
- Independently_Recurrent_Neural_CVPR_2018_paper.html

 [22] J. J. Hopfield, "Neural networks and physical systems with emergent collective computational abilities," Proceedings of the National Academy of Sciences, vol. 79, no. 8, pp. 2554–2558, 1982.

 [Online]. Available: https://www.pnas.org/content/79/8/2554
- [23] H. Ramsauer, B. Schäfl, J. Lehner, P. Seidl, M. Widrich, L. Gruber, M. Holzleitner, M. Pavlović, G. K. Sandve, V. Greiff, D. Kreil, M. Kopp, G. Klambauer, J. Brandstetter, and S. Hochreiter, "Hopfield networks is all you need," in *Submitted* to International Conference on Learning Representations, 2021, under review. [Online]. Available: https://openreview.net/forum?id= tL89RnzIiCd
- [24] A. Howard, M. Sandler, B. Chen, W. Wang, L. Chen, M. Tan, G. Chu, V. Vasudevan, Y. Zhu, R. Pang, H. Adam, and Q. Le, "Searching for mobilenetv3," in 2019 IEEE/CVF International Conference on Computer Vision (ICCV), 2019, pp. 1314–1324.
- [25] J. Gou, B. Yu, S. J. Maybank, and D. Tao, "Knowledge distillation: A survey," CoRR, vol. abs/2006.05525, 2020. [Online]. Available: https://arxiv.org/abs/2006.05525
- [26] L. Deng, G. Li, S. Han, L. Shi, and Y. Xie, "Model compression and hardware acceleration for neural networks: A comprehensive survey," *Proc. IEEE*, vol. 108, no. 4, pp. 485–532, 2020. [Online]. Available: https://doi.org/10.1109/JPROC.2020.2976475
- [27] G. Hinton, O. Vinyals, and J. Dean, "Distilling the knowledge in a neural network," 2015.
- [28] A. Romero, N. Ballas, S. E. Kahou, A. Chassang, C. Gatta, and Y. Bengio, "Fitnets: Hints for thin deep nets," in 3rd International Conference on Learning Representations, ICLR 2015, San Diego, CA, USA, May 7-9, 2015, Conference Track Proceedings, Y. Bengio and Y. LeCun, Eds., 2015. [Online]. Available: http://arxiv.org/abs/1412.6550
- [29] F. Tung and G. Mori, "Similarity-preserving knowledge distillation," in 2019 IEEE/CVF International Conference on

- Computer Vision, ICCV 2019, Seoul, Korea (South), October 27 November 2, 2019. IEEE, 2019, pp. 1365–1374. [Online]. Available: https://doi.org/10.1109/ICCV.2019.00145
- [30] H. Chen, Y. Wang, C. Xu, C. Xu, and D. Tao, "Learning student networks via feature embedding," *IEEE Transactions on Neural Networks and Learning Systems*, vol. 32, no. 1, pp. 25–35, 2021.
- [31] Arm Developer. Neon. [Online]. Available: https://developer. arm.com/architectures/instruction-sets/simd-isas/neon
- [32] Q. Huang, S. K. Zhou, S. You, and U. Neumann, "Learning to prune filters in convolutional neural networks," in 2018 IEEE Winter Conference on Applications of Computer Vision, WACV 2018, Lake Tahoe, NV, USA, March 12-15, 2018. IEEE Computer Society, 2018, pp. 709–718. [Online]. Available: https://doi.org/10.1109/WACV.2018.00083
- [33] Z. Wang, J. Wohlwend, and T. Lei, "Structured pruning of large language models," in *Proceedings of the 2020 Conference on Empirical Methods in Natural Language Processing, EMNLP 2020, Online, November 16-20, 2020, B. Webber, T. Cohn, Y. He, and Y. Liu, Eds. Association for Computational Linguistics, 2020, pp. 6151–6162. [Online]. Available: https://doi.org/10.18653/v1/2020.emnlp-main.496*
- [34] V. Sanh, T. Wolf, and A. M. Rush, "Movement pruning: Adaptive sparsity by fine-tuning," in Advances in Neural Information Processing Systems 33: Annual Conference on Neural Information Processing Systems 2020, NeurIPS 2020, December 6-12, 2020, virtual, H. Larochelle, M. Ranzato, R. Hadsell, M. Balcan, and H. Lin, Eds., 2020. [Online]. Available: https://proceedings.neurips.cc/paper/2020/hash/eae15aabaa768ae4a5993a8a4f4fa6e4-Abstract.html
- [35] S. Han, H. Mao, and W. J. Dally, "Deep compression: Compressing deep neural network with pruning, trained quantization and huffman coding," in 4th International Conference on Learning Representations, ICLR 2016, San Juan, Puerto Rico, May 2-4, 2016, Conference Track Proceedings, Y. Bengio and Y. LeCun, Eds., 2016. [Online]. Available: http://arxiv.org/abs/1510.00149
- [36] H. Yu, S. Edunov, Y. Tian, and A. S. Morcos, "Playing the lottery with rewards and multiple languages: lottery tickets in RL and NLP," in 8th International Conference on Learning Representations, ICLR 2020, Addis Ababa, Ethiopia, April 26-30, 2020. OpenReview.net, 2020. [Online]. Available: https://openreview.net/forum?id=S1xnXRVFwH
- [37] B. Jacob, S. Kligys, B. Chen, M. Zhu, M. Tang, A. G. Howard, H. Adam, and D. Kalenichenko, "Quantization and training of neural networks for efficient integer-arithmetic-only inference," in 2018 IEEE Conference on Computer Vision and Pattern Recognition, CVPR 2018, Salt Lake City, UT, USA, June 18-22, 2018. IEEE Computer Society, 2018, pp. 2704–2713. [Online]. Available: http://openaccess.thecvf.com/content_cvpr_2018/html/Jacob_Quantization_and_Training_CVPR_2018_paper.html
- [38] R. Krishnamoorthi, "Quantizing deep convolutional networks for efficient inference: A whitepaper," CoRR, vol. abs/1806.08342, 2018. [Online]. Available: http://arxiv.org/abs/1806.08342
- [39] V. Klema and A. Laub, "The singular value decomposition: Its computation and some applications," *IEEE Transactions on Automatic Control*, vol. 25, no. 2, pp. 164–176, 1980.
- [40] X. Yu, T. Liu, X. Wang, and D. Tao, "On compressing deep models by low rank and sparse decomposition," in 2017 IEEE Conference on Computer Vision and Pattern Recognition, CVPR 2017, Honolulu, HI, USA, July 21-26, 2017. IEEE Computer Society, 2017, pp. 67–76. [Online]. Available: https://doi.org/10.1109/CVPR.2017.15
- [41] K. Xu, L. Rui, Y. Li, and L. Gu, "Feature normalized knowledge distillation for image classification," in *Computer Vision ECCV* 2020 16th European Conference, Glasgow, UK, August 23-28, 2020, Proceedings, Part XXV, ser. Lecture Notes in Computer Science, A. Vedaldi, H. Bischof, T. Brox, and J. Frahm, Eds., vol. 12370. Springer, 2020, pp. 664–680. [Online]. Available: https://doi.org/10.1007/978-3-030-58595-2_40
- [42] Z. Meng, J. Li, Y. Zhao, and Y. Gong, "Conditional teacher-student learning," in *IEEE International Conference on Acoustics, Speech* and Signal Processing, ICASSP 2019, Brighton, United Kingdom, May 12-17, 2019. IEEE, 2019, pp. 6445–6449. [Online]. Available: https://doi.org/10.1109/ICASSP.2019.8683438
- [43] M. Zhu and S. Gupta, "To prune, or not to prune: Exploring the efficacy of pruning for model compression," in 6th International Conference on Learning Representations, ICLR 2018, Vancouver, BC, Canada, April 30 May 3, 2018, Workshop Track Proceedings. OpenReview.net, 2018. [Online]. Available: https://openreview.net/forum?id=Sy1iIDkPM

- [44] E. Park, J. Ahn, and S. Yoo, "Weighted-entropy-based quantization for deep neural networks," in 2017 IEEE Conference on Computer Vision and Pattern Recognition, CVPR 2017, Honolulu, HI, USA, July 21-26, 2017. IEEE Computer Society, 2017, pp. 7197–7205. [Online]. Available: https://doi.org/10.1109/CVPR.2017.761
- [45] N. Wang, J. Choi, D. Brand, C. Chen, and K. Gopalakrishnan, "Training deep neural networks with 8-bit floating point numbers," in Advances in Neural Information Processing Systems 31: Annual Conference on Neural Information Processing Systems 2018, NeurIPS 2018, December 3-8, 2018, Montréal, Canada, S. Bengio, H. M. Wallach, H. Larochelle, K. Grauman, N. Cesa-Bianchi, and R. Garnett, Eds., 2018, pp. 7686–7695. [Online]. Available: https://proceedings.neurips.cc/paper/2018/ hash/335d3d1cd7ef05ec77714a215134914c-Abstract.html
- [46] R. Banner, I. Hubara, E. Hoffer, and D. Soudry, "Scalable methods for 8-bit training of neural networks," in Advances in Neural Information Processing Systems 31: Annual Conference on Neural Information Processing Systems 2018, NeurIPS 2018, December 3-8, 2018, Montréal, Canada, S. Bengio, H. M. Wallach, H. Larochelle, K. Grauman, N. Cesa-Bianchi, and R. Garnett, Eds., 2018, pp. 5151– 5159. [Online]. Available: https://proceedings.neurips.cc/paper/ 2018/hash/e82c4b19b8151ddc25d4d93baf7b908f-Abstract.html
- [47] W. Wen, C. Xu, F. Yan, C. Wu, Y. Wang, Y. Chen, and H. Li, "Terngrad: Ternary gradients to reduce communication in distributed deep learning," in Advances in Neural Information Processing Systems 30: Annual Conference on Neural Information Processing Systems 2017, December 4-9, 2017, Long Beach, CA, USA, I. Guyon, U. von Luxburg, S. Bengio, H. M. Wallach, R. Fergus, S. V. N. Vishwanathan, and R. Garnett, Eds., 2017, pp. 1509–1519. [Online]. Available: https://proceedings.neurips.cc/paper/2017/ hash/89fcd07f20b6785b92134bd6c1d0fa42-Abstract.html
- [48] A. Paszke, S. Gross, F. Massa, A. Lerer, J. Bradbury, G. Chanan, T. Killeen, Z. Lin, N. Gimelshein, L. Antiga, A. Desmaison, A. Köpf, E. Yang, Z. DeVito, M. Raison, A. Tejani, S. Chilamkurthy, B. Steiner, L. Fang, J. Bai, and S. Chintala, "Pytorch: An imperative style, high-performance deep learning library," in Advances in Neural Information Processing Systems 32: Annual Conference on Neural Information Processing Systems 2019, NeurIPS 2019, December 8-14, 2019, Vancouver, BC, Canada, H. M. Wallach, H. Larochelle, A. Beygelzimer, F. d'Alché-Buc, E. B. Fox, and R. Garnett, Eds., 2019, pp. 8024–8035. [Online]. Available: https://proceedings.neurips.cc/paper/2019/hash/bdbca288fee7f92f2bfa9f7012727740-Abstract.html
- [49] D. Chen, J. Mei, Y. Zhang, C. Wang, Z. Wang, Y. Feng, and C. Chen, "Cross-layer distillation with semantic calibration," CoRR, vol. abs/2012.03236, 2020. [Online]. Available: https://arxiv.org/abs/2012.03236
- [50] N. Passalis, M. Tzelepi, and A. Tefas, "Probabilistic knowledge transfer for lightweight deep representation learning," *IEEE Trans. Neural Networks Learn. Syst.*, vol. 32, no. 5, pp. 2030–2039, 2021. [Online]. Available: https://doi.org/10.1109/TNNLS.2020. 2995884
- [51] Y. Liu, J. Cao, B. Li, C. Yuan, W. Hu, Y. Li, and Y. Duan, "Knowledge distillation via instance relationship graph," in *IEEE Conference on Computer Vision and Pattern Recognition, CVPR* 2019, Long Beach, CA, USA, June 16-20, 2019. Computer Vision Foundation / IEEE, 2019, pp. 7096–7104. [Online]. Available: http://openaccess.thecvf.com/content_CVPR_2019/html/Liu_Knowledge_Distillation_via_Instance_Relationship_Graph_CVPR_2019_paper.html
- [52] Z. Huang and N. Wang, "Like what you like: Knowledge distill via neuron selectivity transfer," CoRR, vol. abs/1707.01219, 2017. [Online]. Available: http://arxiv.org/abs/1707.01219
- [53] A. Gretton, K. M. Borgwardt, M. J. Rasch, B. Schölkopf, and A. Smola, "A kernel two-sample test," J. Mach. Learn. Res., vol. 13, no. 1, p. 723?773, Mar. 2012.
- [54] J. Kim, S. Park, and N. Kwak, "Paraphrasing complex network: Network compression via factor transfer," in Advances in Neural Information Processing Systems 31: Annual Conference on Neural Information Processing Systems 2018, NeurIPS 2018, December 3-8, 2018, Montréal, Canada, S. Bengio, H. M. Wallach, H. Larochelle, K. Grauman, N. Cesa-Bianchi, and R. Garnett, Eds., 2018, pp. 2765– 2774. [Online]. Available: https://proceedings.neurips.cc/paper/ 2018/hash/6d9cb7de5e8ac30bd5e8734bc96a35c1-Abstract.html
- [55] J. D. Hunter, "Matplotlib: A 2d graphics environment," Computing in Science & Engineering, vol. 9, no. 3, pp. 90–95, 2007.
- [56] P. Virtanen, R. Gommers, T. E. Oliphant, M. Haberland, T. Reddy,

- D. Cournapeau, E. Burovski, P. Peterson, W. Weckesser, J. Bright, S. J. van der Walt, M. Brett, J. Wilson, K. J. Millman, N. Mayorov, A. R. J. Nelson, E. Jones, R. Kern, E. Larson, C. J. Carey, İ. Polat, Y. Feng, E. W. Moore, J. VanderPlas, D. Laxalde, J. Perktold, R. Cimrman, I. Henriksen, E. A. Quintero, C. R. Harris, A. M. Archibald, A. H. Ribeiro, F. Pedregosa, P. van Mulbregt, and SciPy 1.0 Contributors, "SciPy 1.0: Fundamental Algorithms for Scientific Computing in Python," *Nature Methods*, vol. 17, pp. 261–272, 2020.
- [57] C. R. Harris, K. J. Millman, S. J. van der Walt, R. Gommers, P. Virtanen, D. Cournapeau, E. Wieser, J. Taylor, S. Berg, N. J. Smith, R. Kern, M. Picus, S. Hoyer, M. H. van Kerkwijk, M. Brett, A. Haldane, J. Fernández del Río, M. Wiebe, P. Peterson, P. Gérard-Marchant, K. Sheppard, T. Reddy, W. Weckesser, H. Abbasi, C. Gohlke, and T. E. Oliphant, "Array programming with NumPy," Nature, vol. 585, p. 357–362, 2020.
- [58] F. Pérez and B. E. Granger, "Ipython: A system for interactive scientific computing," Comput. Sci. Eng., vol. 9, no. 3, pp. 21–29, 2007. [Online]. Available: https://doi.org/10.1109/MCSE.2007.53
- [59] Wes McKinney, "Data Structures for Statistical Computing in Python," in Proceedings of the 9th Python in Science Conference, Stéfan van der Walt and Jarrod Millman, Eds., 2010, pp. 56 – 61.
- [60] T. pandas development team, "pandas-dev/pandas: Pandas," Feb. 2020. [Online]. Available: https://doi.org/10.5281/zenodo. 3509134
- [61] F. Pedregosa, G. Varoquaux, A. Gramfort, V. Michel, B. Thirion, O. Grisel, M. Blondel, P. Prettenhofer, R. Weiss, V. Dubourg, J. Vanderplas, A. Passos, D. Cournapeau, M. Brucher, M. Perrot, and Édouard Duchesnay, "Scikit-learn: Machine learning in python," *Journal of Machine Learning Research*, vol. 12, no. 85, pp. 2825–2830, 2011. [Online]. Available: http://jmlr.org/papers/v12/pedregosa11a.html
- [62] R. Müller, S. Kornblith, and G. E. Hinton, "When does label smoothing help?" in Advances in Neural Information Processing Systems 32: Annual Conference on Neural Information Processing Systems 2019, NeurIPS 2019, December 8-14, 2019, Vancouver, BC, Canada, H. M. Wallach, H. Larochelle, A. Beygelzimer, F. d'Alché-Buc, E. B. Fox, and R. Garnett, Eds., 2019, pp. 4696–4705. [Online]. Available: http://papers.nips.cc/paper/8717-when-does-label-smoothing-help
- [63] J. L. Reyes-Ortiz, L. Oneto, A. Samà, X. Parra, and D. Anguita, "Transition-aware human activity recognition using smartphones," *Neurocomputing*, vol. 171, pp. 754–767, 2016. [Online]. Available: https://doi.org/10.1016/j.neucom.2015.07.085
- [64] D. Anguita, A. Ghio, L. Oneto, X. Parra, and J. L. Reyes-Ortiz, "A public domain dataset for human activity recognition using smartphones," in 21st European Symposium on Artificial Neural Networks, ESANN 2013, Bruges, Belgium, April 24-26, 2013, 2013. [Online]. Available: http://www.elen.ucl.ac.be/ Proceedings/esann/esannpdf/es2013-84.pdf
- [65] K. Altun, B. Barshan, and O. Tunçel, "Comparative study on classifying human activities with miniature inertial and magnetic sensors," *Pattern Recognit.*, vol. 43, no. 10, pp. 3605–3620, 2010. [Online]. Available: https://doi.org/10.1016/j.patcog.2010.04.019
- [66] B. Barshan and M. C. Yüksek, "Recognizing daily and sports activities in two open source machine learning environments using body-worn sensor units," *Comput. J.*, vol. 57, no. 11, pp. 1649–1667, 2014. [Online]. Available: https://doi.org/10.1093/ comjnl/bxt075
- [67] K. Áltun and B. Barshan, "Human activity recognition using inertial/magnetic sensor units," in *Human Behavior Understanding*, First International Workshop, HBU 2010, Istanbul, Turkey, August 22, 2010. Proceedings, ser. Lecture Notes in Computer Science, A. A. Salah, T. Gevers, N. Sebe, and A. Vinciarelli, Eds., vol. 6219. Springer, 2010, pp. 38–51. [Online]. Available: https://doi.org/10.1007/978-3-642-14715-9_5
- [68] O. Baños, M. Damas, H. Pomares, I. Rojas, M. A. Tóth, and O. Amft, "A benchmark dataset to evaluate sensor displacement in activity recognition," in *The 2012 ACM Conference on Ubiquitous Computing, Ubicomp '12, Pittsburgh, PA, USA, September 5-8, 2012, A. K. Dey, H. Chu, and G. R. Hayes, Eds. ACM, 2012, pp. 1026–1035.* [Online]. Available: https://doi.org/10.1145/2370216.2370437
- [69] O. Baños, M. A. Tóth, M. Damas, H. Pomares, and I. Rojas, "Dealing with the effects of sensor displacement in wearable activity recognition," *Sensors*, vol. 14, no. 6, pp. 9995–10 023, 2014. [Online]. Available: https://doi.org/10.3390/s140609995

- [70] H. Yong, J. Huang, X. Hua, and L. Zhang, "Gradient centralization: A new optimization technique for deep neural networks," in Computer Vision ECCV 2020 16th European Conference, Glasgow, UK, August 23-28, 2020, Proceedings, Part I, ser. Lecture Notes in Computer Science, A. Vedaldi, H. Bischof, T. Brox, and J. Frahm, Eds., vol. 12346. Springer, 2020, pp. 635–652. [Online]. Available: https://doi.org/10.1007/978-3-030-58452-8_37
- [71] F. Tung and G. Mori, "Similarity-preserving knowledge distillation," in 2019 IEEE/CVF International Conference on Computer Vision, ICCV 2019, Seoul, Korea (South), October 27 November 2, 2019. IEEE, pp. 1365–1374. [Online]. Available: https://doi.org/10.1109/ICCV.2019.00145



Runze Chen received the B.S. degree from the School of Software Engineering, Beijing University of Posts and Telecommunications, Beijing, China, in 2019. He is working toward the Ph.D. degree in Beijing University of Posts and Telecommunications and is a visiting student in the Institute of Computer Technology, Chinese Academy. His research interests include: mobile computing, autonomous vehicles and mobile intelligence.



Haiyong Luo received the B.S. degree from the Department of Electronics and Information Engineering, Huazhong University of Science and Technology, Wuhan, China, in 1989, the M.S. degree from the School of Information and Communication Engineering, Beijing University of Posts and Telecommunication, China, in 2002, and the Ph.D. degree in computer science from the University of Chines Academy of Sciences, Beijing, China, in 2008. He is currently an Associate Professor with the Institute of Computer

Technology, Chinese Academy of Science, China. His main research interests are location-based services, pervasive computing, mobile computing, and Internet of Things. He is a member of the IEEE.



Fang Zhao received the B.S. degree from the School of Computer Science and Technology, Huazhong University of Science and Technology, Wuhan, China, in 1990, the M.S. and Ph.D. degrees in computer science and technology from the Beijing University of Posts and Telecommunications, Beijing, China, in 2004 and 2009, respectively. She is currently a Professor with the School of Software Engineering, Beijing University of Posts and Telecommunication. Her research interests include mobile computing,

location-based services, and computer networks.



Xuechun Meng received the B.S. degree from the School of Computer science and Technology, China University of Mining and Technology, Jiangsu, China, in 2020. She is currently studying in Beijing University of Posts and Telecommunications and is a visiting student in the Institute of Computer Technology, Chinese Academy. Her interests include: simultaneous localization and mapping, semantic segmentation.



Zhiqing Xie received the B.S. degree from the School of Computer Science and Technology, China University of Mining and Technology, Jiangsu, China, in 2020. He is working toward the M.S. degree in Beijing University of Posts and Telecommunications and is a visiting student in the Institute of Computer Technology, Chinese Academy. His research interests include: mobile computing and mobile intelligence.



machine learning.

Yida Zhu received the B.S. degree in soft engineering from the School of Software Engineering, Beijing University of Posts and Telecommunications, Beijing, China, in 2017. He is currently pursuing the Ph.D. degree with the School of Software Engineering, Beijing University of Posts and Telecommunications, and is a visiting student in the Institute of Computer Technology, Chinese Academy. His current main interests include location-based services, pervasive computing, deep learning, transfer learning, and